



Degree Project in *Electrical Engineering, Specialising in Systems, Control and Robotics*

Second Cycle, 30 credits

Extended Kalman Filter as Observer for a Hydrofoiling Watercraft

Modelling of a new hydrofoiling concept, based on the Spherical Inverted Pendulum Model

ADAM THÅLIN

Sammanfattning

Principen för bärplan är att generera lyftkraft från vattnet på samma sätt som flygplansvingar genererar lyftkraft från luften för att lyfta farkostens skrov ur vattnet. Detta minskar motståndet från friktionen mellan skrov och vatten vilket möjliggör snabbare och jämnare transport på vatten med en lägre energiförbrukning än traditionella planande skrov. På senare år har tekniken fått ett uppsving i och med framsteg inom strömningsmekanik, reglerteknik och materiallära. Detta i takt med datorers ökande beräkningskraft har lett till att bärplanskonstruktioner har kunnat uppvisa en överlägsenhet i vattensporter som kappsegling och surfing när det kommer till fart och komfort.

Forskare och studenter på avdelningen för farkostteknik och solidmekanik vid Kungliga Tekniska Högskolan, Stockholm arbetar med att ta fram en ny typ av farkost med en minimal bärplansdesign, FoilCart. Dess utformning gör att det mekaniska beteendet kan liknas vid en inverterad pendel, vilket är ett välkänt, olinjärt reglerproblem som kan lösas på flera sätt. Denna avhandling är ett vidarearbete som bygger på en modell med fyra frihetsgrader från en tidigare avhandling kring FoilCart-projektet. Modellen med fyra frihetsgrader var, på grund av förenklingar och linjärisering av systemdynamiken, bristfällig och kunde inte garantera en robust balansering av farkosten förutom i linjäriseringspunkten. Modellen som presenteras i denna avhandling har sex frihetsgrader. Mekaniken och systemdynamiken härleds från den sfäriska inverterade pendeln tillsammans med styrningen från bärplansmodulen, utan förenklingar och linjärisering. Modellen används i ett Kalmanfilter för att konstruera en observatör för tillståndsrekonstruktion.

Den framtagna modellen valideras med en FoilCart-modell i Simulink. Resultaten visar att observatören kan ge en noggrann tillståndsrekonstruktion även vid simulerat mätbrus i mätsignalen. Avhandlingen syftar till att visa hur den inverterade pendelmodellen kan användas vid framtida implementation av rekonstruerad tillståndsåterkoppling.

I och med avgränsningar i avhandlingen finns det också en del strömningsmekaniska aspekter som inte tagits med vid framtagningen av denna modell. Eftersom farkosten delvis är omgiven av vatten och delvis av luft skulle det vara intressant att undersöka om noggrannheten i tillståndsrekonstruktionen kan förbättras genom att använda avancerad strömningsmekanik.

Nyckelord

Bärplan, Extended Kalman Filter, Farkostteknik, Inverterad Pendel, Sensorfusion, Sex frihetsgrader, Simulink

Abstract

Hydrofoiling in general has the potential to revolutionize watercraft in the future since it allows smoother and faster transport on water with less energy consumption than traditional planning hulls. Even if the concept of hydrofoiling has been around since the last century, development in control theory and material science together with increased computing power has led to a growing interest for the technology. Especially in water sports such as speed sailing and surfing due to its superiority in speed and comfort.

Researchers and students at the Engineering Mechanics Department at KTH, Royal Institute of Technology, Stockholm are working on a new type of watercraft, utilizing only one single hydrofoil with the intention to minimize drag for faster and smoother rides in various wave and weather conditions.

The difficulties lie in understanding the relationship between actuators and the mechanics. This thesis is a continuation work from a previous thesis which designed a control strategy based on a model with 4 degrees of freedom (DOF). Due to simplifications and linearizations, the 4 DOF model was not rich enough to meet the performance requirements.

This thesis presents a 6 DOF model by deriving the mechanical equations for the spherical inverted pendulum and actuation from the hydrofoiling module. The inverted pendulum model is a well-known control problem that can be solved with different strategies. By showing that the hydrofoiling concept can be modelled as an inverted pendulum, it is also shown that it can be controlled as an inverted pendulum.

The derived model is used together with an Extended Kalman Filter to create an observer. The observer is validated with a spherical inverted pendulum model in Matlab and the block diagram environment, Simulink. Simulation results show that the 6 DOF model is able to produce accurate state estimation of the watercraft even in the presence of stochastic measurement noise.

It is also concluded that viscous forces, that arise from the watercraft being partly surrounded by water and partly by air, need further investigation.

Keywords

Extended Kalman Filter, Hydrofoiling, Spherical Inverted Pendulum, Sensor Fusion, Simulink

Acknowledgements

I would like to thank all the people involved in the FoilCart project. Special thanks to supervisor Ivan Stenius for helping me with knowledge and understanding in naval architecture, and Nicholas Honeth for providing knowledge and insight in the FoilCart's sensors and micro-controllers.

Great thanks to all members of Tribologikommisionen too, for fruitful discussions and interesting viewpoints on engineering related topics.

Finally, I would like to thank some people at the Division of Computational Science and Technology at KTH, Royal Institute of Technology. Especially my examiner Stefano Markidis, my supervisor Kateryna Morozovska and Federica Bragone for fruitful discussions and guidance in academic writing.

Contents

| | | |
|----------|--|-----------|
| 1 | Introduction | 1 |
| 1.1 | Problem description | 1 |
| 1.1.1 | Original Problem | 1 |
| 1.1.2 | Scientific and Engineering issues | 2 |
| 1.2 | Purpose | 2 |
| 1.3 | Goals | 2 |
| 1.4 | Research Methodology | 3 |
| 1.5 | Delimitation and scope | 3 |
| 1.6 | Ethical considerations | 3 |
| 2 | Background | 5 |
| 2.1 | Hydrofoiling | 5 |
| 2.2 | History of hydrofoils | 5 |
| 2.3 | Types of hydrofoils | 6 |
| 2.4 | Parameter estimation | 8 |
| 2.4.1 | Extended Kalman Filter | 8 |
| 2.5 | Disturbance rejection | 9 |
| 2.5.1 | Low-pass filter | 9 |
| 2.6 | Discretization | 9 |
| 3 | Method | 13 |
| 3.1 | Models | 13 |
| 3.1.1 | Inverted pendulum on a cart | 13 |
| 3.1.2 | Spherical inverted pendulum model in 4 DOF | 14 |
| 3.1.3 | Spherical inverted pendulum model in 5 DOF | 15 |
| 3.1.4 | Spherical inverted pendulum model in 6 DOF | 16 |
| 3.2 | State space | 17 |
| 4 | Implementation | 21 |
| 4.1 | Simulink model | 21 |
| 4.2 | Modelling | 23 |
| 4.2.1 | Lagrangian mechanics | 23 |
| 4.2.2 | Newtonian mechanics | 24 |
| 4.3 | Extended Kalman Filter | 28 |
| 4.4 | Sensor fusion | 29 |
| 5 | Results | 31 |
| 5.1 | Pitch case | 31 |
| 5.1.1 | Perfect states | 31 |
| 5.1.2 | Estimated states | 32 |

| | | |
|----------|--|-----------|
| 5.1.3 | Scaling the dimensions to slow down system dynamics in observer system | 33 |
| 5.1.4 | Tuning the EKF | 34 |
| 5.1.5 | Sinusoidal disturbance | 35 |
| 5.1.6 | Lowpass-filter | 37 |
| 5.1.7 | White noise disturbance | 38 |
| 5.1.8 | Altitude estimation | 40 |
| 5.2 | Roll case | 41 |
| 5.2.1 | Perfect states | 42 |
| 5.2.2 | Estimated states | 42 |
| 5.3 | Yaw case | 43 |
| 5.3.1 | Perfect states | 43 |
| 5.3.2 | Estimated states | 44 |
| 5.4 | Discussion | 45 |
| 6 | Conclusion and Future Work | 47 |
| 6.1 | Conclusion | 47 |
| 6.2 | Future work | 47 |

List of Tables

| | | |
|-----|---|----|
| 4.1 | Parameters used calculate lift and drag forces in Figure 4.2. | 23 |
| 4.2 | Parameters used to derive the 6 DOF model. | 26 |

LIST OF TABLES

List of Figures

| | | |
|------|--|----|
| 2.1 | Image of a boat using U-shaped surface-piercing hydrofoiling. [1] | 6 |
| 2.2 | Image of a Candela C-8 equipped with fully submerged hydrofoils. [2] . | 7 |
| 2.3 | Prototype design of the FoilCart at Maritime Robotics Lab (MRL). [3] . | 7 |
| 3.1 | Demonstration of the inverted pendulum on a cart-model in 2 DOF. [3] | 14 |
| 3.2 | Spherical inverted pendulum model in 4 DOF. [3] | 14 |
| 3.3 | Visualization of Euler angles used to describe the orientation of an aircraft. α - Yaw, β - pitch and γ - roll. [4] | 15 |
| 3.4 | 5 DOF model of inverted pendulum or pendulum on a cart in space. [5] | 16 |
| 3.5 | The 6 DOF model, using three frames of reference. $OXYZ$ as fixed frame, $O'xyz$ parallel to the fixed frame with origin at the IMU and $O'x'y'z'$ as the IMU coordinate system. | 17 |
| 4.1 | Plant system block. | 22 |
| 4.2 | Observer system in Simulink. | 22 |
| 4.3 | Top level view of the Simulink model with observer system attached to the loop. | 23 |
| 4.4 | Input modelling. | 25 |
| 4.5 | Dimensions of input modelling. | 26 |
| 4.6 | Altitude data from a test ride with the full scale prototype. The blue lines are altitude data from sonars in the aft and the fore. The red line is speed. | 29 |
| 4.7 | Two dimensional trigonometry for calculating the altitude using sensor fusion. θ is the angle between the axis perpendicular to Earth and the IMU's z-axis. | 30 |
| 5.1 | Simulation output considered as perfect states, unaffected by disturbances. | 32 |
| 5.2 | Observer states with no disturbance | 33 |
| 5.3 | A wench that shows how the torque in the red dot can be changed by modifying the distance from the red dot to the point of force application, (r in (4.17)). | 34 |
| 5.4 | Observer states with no disturbance. Dimensions scaled by a factor 1/1000. | 34 |
| 5.5 | Observer states with no disturbance. EKF tuned with $Q_k = 2I_{12}$ and $R_k = I_{12}$ to put more weight on the measured output rather than the output from the model. | 35 |
| 5.6 | Measurement with sinusoidal disturbance. | 36 |
| 5.7 | Observer states with sinusoidal disturbance. | 37 |
| 5.8 | Lowpass-filtered observer states with sinusoidal disturbance. | 38 |
| 5.9 | Measurement with white noise disturbance. | 39 |
| 5.10 | EKF output in presence of white noise disturbance with tuning parameters $Q = 8I_{12}$ and $R = 7I_{12}$ | 40 |

| | | |
|------|--|----|
| 5.11 | Estimation of the altitude with EKF. | 41 |
| 5.12 | Altitude estimation with EKF parameters $Q = I_{12}$ and $R = 8I_{12}$ in the presence of white noise disturbance. | 41 |
| 5.13 | Perfect states for roll case without disturbance. | 42 |
| 5.14 | Observer states for roll case without disturbance. | 43 |
| 5.15 | Perfect states for yaw case without disturbance. | 44 |
| 5.16 | Observer states for yaw case without disturbance. | 45 |

List of Abbreviations

CFD Computational Fluid Dynamics

CPU Central Processing Unit

DOF Degrees of freedom

EKF Extended Kalman Filter

GPS Global Positioning System

Hz Hertz

IMU Inertial Measurement Unit

kph Kilometers per hour

kts Knots

LQR Linear Quadratic Regulator

MRL Maritime Robotics Lab

PID Controller Proportional, Integrating, Differentiating controller

PWM Pulse Width Modulation

s Second(s)

Chapter 1

Introduction

Hydrofoiling technique is often associated with water sports such as speed sailing and surfing due to its proven superiority in speed and comfort. In a similar way that airplane wings are used to lift airplanes off the ground, hydrofoils are used to lift a boat's hull above the water. The amount of water that needs to be displaced is therefore decreased as well as the friction between hull and water.

The advantages of hydrofoiling over traditional planning hulls cannot only be used for recreational purposes such as sport and competition. Minimizing the drag forces between hull and water could make it possible to replace fossil fueled engines with electric motors without losing range or speed. Hydrofoiling therefore has the potential to be revolutionizing in the process of making the boating industry fossil free for a sustainable future.

The department of Engineering Mechanics at Royal Institute of Technology, KTH in Stockholm is in the process of developing a new type of watercraft with a minimalist hydrofoiling module. The prototype is called FoilCart and is a full scale model equipped with several micro computers and sensors.

1.1 Problem description

There are essentially two sides of the problem. The first is geared towards engineering since it is about guaranteeing stable rides on water. The other is of scientific character and is about the investigation of how and if the hydrofoiling concept can be modelled as an inverted pendulum.

1.1.1 Original Problem

The balancing of the watercraft can be considered as an inverted pendulum, similar to trying to balance a broom on the hand.

In [3], a model based on the inverted pendulum is derived by superpositioning the system into two systems that are controlled separately with PID controllers. A PID controller is one most widely used controllers since it is able to provide sufficient performance in a variety of applications despite its low complexity.

It has been shown that a hovering quadrotor can balance an inverted pendulum by using relatively primitive control strategies such as PID control in [6]. Linearization and assumptions that some angles are fixed are however not robust enough for this problem when disturbances come from water. Due to chemical differences between air and water, aerial disturbances like indoor wind gusts do not contain as much disturbance energy as for example a water wave.

There are generally two ways of dealing with a wave when riding a boat. The first is ride on top of the wave, which is most suitable for larger waves and can be compared to going over a hill with a road vehicle as opposed to going through the hill. The other is to break the wave and ride through it, similar to active suspension in road vehicles when riding on a rocky road. The road is bumpy, but the passengers do not experience the shape of the road. In order to spare the passengers from feeling the shape of the wave by going through it, an observer like for example a Kalman Filter is needed. It works by defining a plane to ride on rather than the shape of the water.

1.1.2 Scientific and Engineering issues

The inverted pendulum on a cart is often used as an example of a system with nonlinear system dynamics. It is therefore also commonly used in education and for benchmarking nonlinear control strategies.

Since it is a well-known control problem with several solutions, it is of interest to investigate if the hydrofoiling concept can be modelled as an inverted pendulum. If it is possible, there is already a variety of strategies that can be used balance the hydrofoiling concept.

The core of this thesis is to model the watercraft as a six degrees of freedom (6 DOF) inverted pendulum. Some outputs of the system are affected by the same input signal, which means that the system also is input-output coupled. Such effects are also desired to be included in the model.

In some cases, linear methods are able to provide sufficient robustness. In other cases, there are often reasons to use nonlinear methods as for example when:

- System contains strong nonlinearities that cannot be accurately approximated with a linear system.
- There exists multiple equilibria.
- Performance is critical and needs to be pushed to the limit.

In this case, it is the performance which is the major reason to investigate nonlinear control methods. If it is shown that the inverted pendulum model is an accurate representation of the watercraft, it has the potential to be used for observer design control which means that the controller acts on information from the observer rather than the direct measurements. Observer design control is an important step towards guaranteeing smooth rides in wavy waters.

1.2 Purpose

The purpose of this thesis is to investigate how and if the inverted pendulum model can be used for accurate state estimation of a hydrofoiling watercraft that uses a super compact hydrofoiling module.

Solutions to the inverted pendulum control problem already exists, so showing that the hydrofoiling concept can be modelled as an inverted pendulum means that the hydrofoiling concept's control problem can be solved.

1.3 Goals

The goal of this thesis is to answer the question if a hydrofoiling watercraft with super compact hydrofoiling module can be modelled as an inverted pendulum.

More specifically, the goals are:

- Using the spherical inverted pendulum model to derive a model of a hydrofoiling watercraft.
- Show how an Extended Kalman Filter (EKF) based on a 6 DOF inverted pendulum model can be used as an observer for a hydrofoiling watercraft with super compact hydrofoiling module.

1.4 Research Methodology

The idea for this thesis is to use the 4 DOF model from [3] and increase the complexity such that rotation around and movement along the vertical axis are also included.

In this thesis, modelling should be done without linearizing or ignoring degrees of freedom such that the choice of control strategy is not limited to linear controllers. Since I have a background in mechanics, the model will be derived using classical mechanics and rigid body kinematics.

Given the available knowledge and software, the implementation will be done in Matlab and its block diagram environment, Simulink.

1.5 Delimitation and scope

This project will not focus on the fluid dynamics or material science of the hydrofoiling structure. The control strategy will need to take physical limitations of the testing platform in consideration since this thesis does not include any re-design or re-build of the hydrofoiling structure.

The hydrofoiling watercraft has similarities to a fighter jet in the sense that it requires active control when "flying". Because of that, it can be tempting to try to incorporate some of the concepts that are proven to work for the aircraft. It was discovered in the pre-study that aircraft control is a branch of its own which has been developed over a long time. It must however not be forgotten that this thesis focuses on the 6 DOF inverted pendulum model. Aircraft control could be interesting in the future but by not choosing aircraft control from the start, it should not be done later in this thesis either since it is conflicting with the inverted pendulum model.

1.6 Ethical considerations

Confirmation bias is a threat against the ethics of this thesis project. Consciously or unconsciously misinterpreting the results to create a distorted conclusion in order to display the concept as more successful than it really is. By investigating how the performance can be improved, it must not be forgotten that there is a possibility that performance cannot be improved with the methods used in the thesis. The FoilCart team and the stakeholders are driven by success so from a scientific standpoint it is important to only look at the results we get, not the results we want.

Chapter 2

Background

This section aims to provide a general introduction to different types of the hydrofoiling technique. The main idea is described briefly followed by the historical role of hydrofoiling.

2.1 Hydrofoiling

Hydrofoils are a type of wing mounted under the hull of a watercraft. As the watercraft gains speed, the wing creates lift from the water in the same way as airplanes create lift from the air. This causes the entire watercraft to be lifted above the water surface, removing the friction between hull and water. The inspiration for this new minimalist hydrofoiling concept comes from surfboard hydrofoils.

The technology has become popular with the development of electric boats and improved possibilities for automatic control of the hydrofoil. Advancements in material science and computational fluid dynamics (CFD) have also contributed to its increased popularity.

2.2 History of hydrofoils

As early as 1908, Alexander Graham Bell, also known as the inventor of the telephone, developed along with his wife, Mabel Bell, and his colleague, Frederick W. Baldwin, the first hydrofoil equipped vessel, the "Hydrodrome". [7] In September, 1919, their hydrofoil equipped vessel, HD-4 (fourth iteration of the Hydrodrome) reached a whopping speed of 114 kph [7], which was faster than any human had travelled on water before. The fastest steamships at the time could reach speeds around 60 kph. [7]

In recent years, hydrofoiling technique has seen an increase in popularity thanks to development in simulation technology and material science. Nowadays, hydrofoiling is a common sight in water sports such as speed sailing and surfing due to its superiority in speed and comfort.

In 2012, Emirates Team from New Zealand brought hydrofoiling to the America's Cup and changed the face of top-level yacht racing forever. The AC75 class in America's Cup is a class exclusively for hydrofoiling sailboats. [8] Apart from basic rules governing dimensions and weight, the hydrofoiling design is open territory for designers and engineers. [9]

2.3 Types of hydrofoils

Hydrofoils come in many shapes and are often categorized as surface-piercing or fully submerged hydrofoils. Surface-piercing hydrofoils as seen in Figure 2.1 are, as the name suggests, only partially under water [3]. Since the foil has the same shape as the hull, it is self-stabilizing like an low-winged aircraft [10].

Fully submerged hydrofoils as seen in Figure 2.2 are more similar to a high-winged or parasol-winged aircraft [10] in terms of stability. In contrast to the surface piercing hydrofoils, they are not self-stabilizing and require active control to remain stable. The foils are often shaped as upside down letter "T".



Figure 2.1: Image of a boat using U-shaped surface-piercing hydrofoiling. [1]



Figure 2.2: Image of a Candela C-8 equipped with fully submerged hydrofoils. [2]

The type that is mounted on the FoilCart is a fully submerged hydrofoil similar to the Candela C-8 in Figure 2.2. The FoilCart design can be seen in Figure 2.3. A noticeable difference between the FoilCart's hydrofoiling concept and the C-8's is that the FoilCart has one mast compared to three on the C-8.

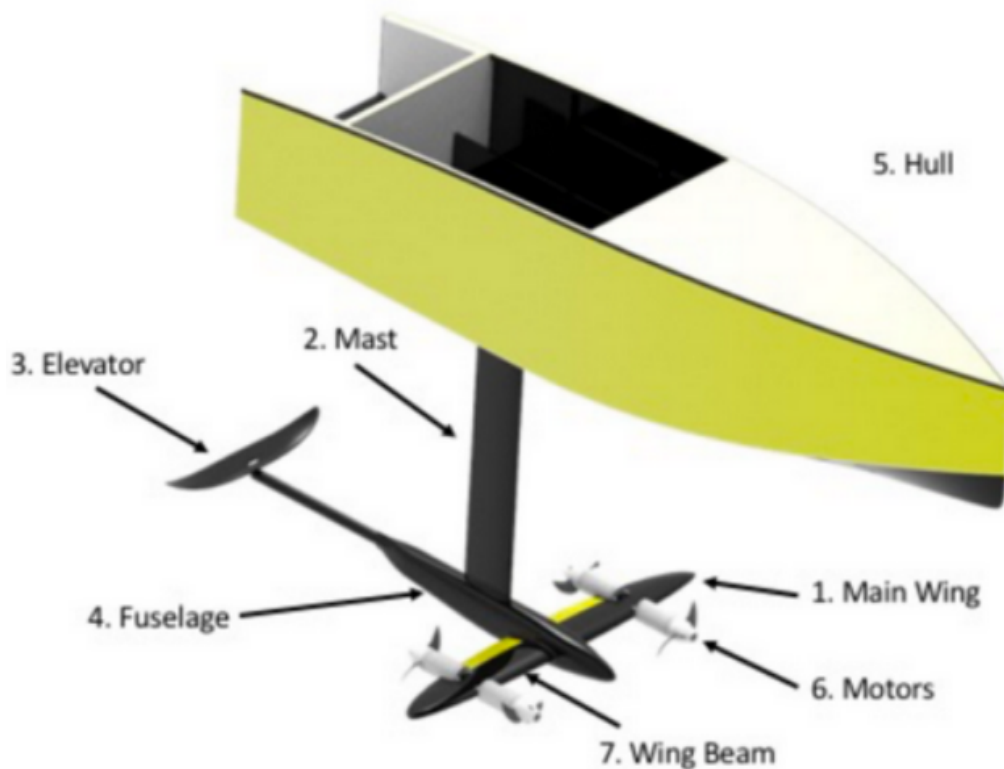


Figure 2.3: Prototype design of the FoilCart at Maritime Robotics Lab (MRL). [3]

2.4 Parameter estimation

Not all state variables will be measured and available for feedback. Kalman filter is mentioned in [3] as a method of state estimation based on sensor inputs. A Kalman filter is an algorithm used to estimate states of a dynamical system with noisy and incomplete measurements. It combines the noisy and incomplete measurements with output from a model of the system to create an estimate of the system state in every time step.

2.4.1 Extended Kalman Filter

There are several variations of the Kalman filter and they are designed for different purposes. Since the inverted pendulum is a nonlinear system, the Extended Kalman filter (EKF) is a suitable variation since it is one of the most widely used methods for estimating systems with nonlinear dynamics. [11]

Consider the discrete and nonlinear system

$$x[k] = f(x[k-1], u[k]) + w[k] \quad (2.1)$$

$$y[k] = h(x[k]) + v[k] \quad (2.2)$$

with process noise $w[k] \sim \mathcal{N}(0, Q_k)$ and $v[k] \sim \mathcal{N}(0, R_k)$. The EKF iterates in two steps; first predict and then update.

Predict

In the predict step, a prediction of the states based on the control input to the observer system is computed. A prediction of the covariance estimate P_k is also computed here. Estimated state variables are commonly denoted with a hat. For example, $\hat{x}[k|k-1]$ denotes the estimate at time k given observations in time $k-1$. The Predict step consists of the following expressions:

$$\hat{x}[k|k-1] = f(\hat{x}[k-1|k-1], u[k]) \quad (2.3)$$

$$P_{k|k-1} = A_k P_{k-1|k-1} A_k^T + Q_k, \quad (2.4)$$

where

$$A_k = \frac{\partial}{\partial x} f(\hat{x}_k, u). \quad (2.5)$$

Update

The update step works to correct the prediction from the predict step based on the error between the prediction and the measurement.

The update step consists of the following steps with a short description in the paragraph below:

$$\tilde{y}[k] = y[k] - h(\hat{x}[k|k-1]) \quad (2.6)$$

$$S_k = C_k P_{k|k-1} C_k^T + R_k \quad (2.7)$$

$$K_k = P_{k|k-1} C_k^T S_k^{-1} \quad (2.8)$$

$$\hat{x}[k|k] = \hat{x}[k|k-1] + K_k \tilde{y}[k] \quad (2.9)$$

$$P_{k|k} = (I - K_k C_k) P_{k|k-1} \quad (2.10)$$

where

$$C_k = \frac{\partial}{\partial x} h(\hat{x}_k). \quad (2.11)$$

The measurement residual (2.6) is computed as well as the residual covariance (2.7) and Kalman gain (2.8). The Kalman gain is then used to correct the prediction of the states (2.9) and the covariance estimate (2.10).

Due to the use of the Jacobians (2.5) and (2.11), the prediction of the state estimate is only a linear approximation of the true prediction. Unless the system is linear, the EKF is not an optimal observer. Despite that, the EKF is still de facto standard in navigation systems and GPS due to its ability to perform reasonably well as a real-time state estimator for nonlinear systems. [12]

2.5 Disturbance rejection

There are two types of disturbance that has to be taken into consideration. One is process noise that comes from wind and irregularities on the water surface. The other is measurement noise that comes from perturbations in sensors.

2.5.1 Low-pass filter

In addition to the EKF, a low-pass filter

$$x_{filtered}(t_k) = \frac{T_f}{T_f + h} x_{filtered}(t_{k-1}) + \frac{h}{T_f + h} x_{measured}(t_k) \quad (2.12)$$

where T_f is the filter time constant and $h = t_k - t_{k-1}$ is the sampling time, can be implemented to filter out high frequency content from the sensor data if we have reasons to believe that it is disturbance. By increasing T_f , the cutoff frequency

$$f_c = \frac{1}{2\pi} \frac{1}{T_f} \quad [\text{Hz}] \quad (2.13)$$

is lowered and the bandwidth $f_B = f_c$ is narrowed which means that the filtered signal will have less high frequency content. To successfully filter out frequencies in the sensor data, the filter time constant should be considerably larger than the sampling time since the highest frequency that can be sampled with the sampling time h is $\frac{1}{2h}$ Hz. According to [13], $h < \frac{T_f}{5}$ is a good practice to ensure that the filter behaves as the continuous low-pass filter that it is derived from.

2.6 Discretization

One thing that is mentioned but not shown in [3] is discretization. All modelling in [3] is expressed in continuous time domain. Differential equations have the potential to hold more physical information than equations of difference, but the downside is that a continuous system relies on the assumption that an infinite number of actions are possible in one time step, which is not the case when using a digital controller. The controller on the FoilCart is digital and since one of the goals is to improve the robustness, control design should be done in discrete-time domain. To discretize the system, the sample and hold method can be used [14], as described below.

Consider a continuous state space model on the form

$$\dot{x}(t) = A_c x(t) + B_c u(t) \quad (2.14)$$

$$y = Cx(t) + Du(t). \quad (2.15)$$

The discrete system equivalent to (2.14), (2.15) obtained with the sample and hold method is then

$$x[kh + h] = \underbrace{e^{A_c h}}_{A_d} x[kh] + \underbrace{\int_{s=0}^h e^{A_c s} B_c ds}_{B_d} u[kh] \quad (2.16)$$

$$y[k] = Cx[k] + Du[k] \quad (2.17)$$

where $e^{A_c h}$ is the matrix exponential of A_c with sampling time h . This is a way to rewrite the state equations as equations of difference instead of differential equations. Equations of difference does not hold as much physical information as differential equations but they are more suitable for digital controllers as the delay from the sampling time is taken into consideration.

Chapter 3

Method

This chapter aims to present the underlying theory used in the derivation of the 6 DOF model and the implementation of the observer.

3.1 Models

This section aims to give an introduction of the inverted pendulum model. The models are essentially the same system but with different levels of complexity.

3.1.1 Inverted pendulum on a cart

The inverted pendulum on a cart model Figure 3.1 is one of the simplest nonlinear systems with an unstable equilibrium. Even though it only includes two degrees of freedom, the system is often used as an example of nonlinear systems in education and benchmarking of feedback control systems.

When the FoilCart is in a flying state with the hull above the water surface, it shows similar unstable behavior as the inverted pendulum on a cart. This makes it possible to control the pitch of the FoilCart in the same way as the inverted pendulum on a cart.

However, since the FoilCart operates in three dimensions, there are more angles that need to be controlled when balancing the vessel. For example, the roll can also be controlled as an inverted pendulum on a cart.

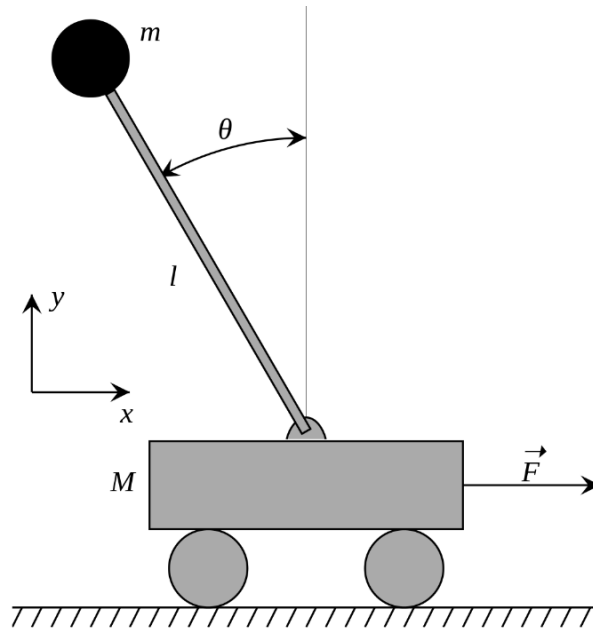


Figure 3.1: Demonstration of the inverted pendulum on a cart-model in 2 DOF. [3]

3.1.2 Spherical inverted pendulum model in 4 DOF

Two inverted pendulum on a cart systems with 2 DOF can be combined with the superposition principle to create a system with 4 DOF. This is a part of the solution to the control problem shown in [3].

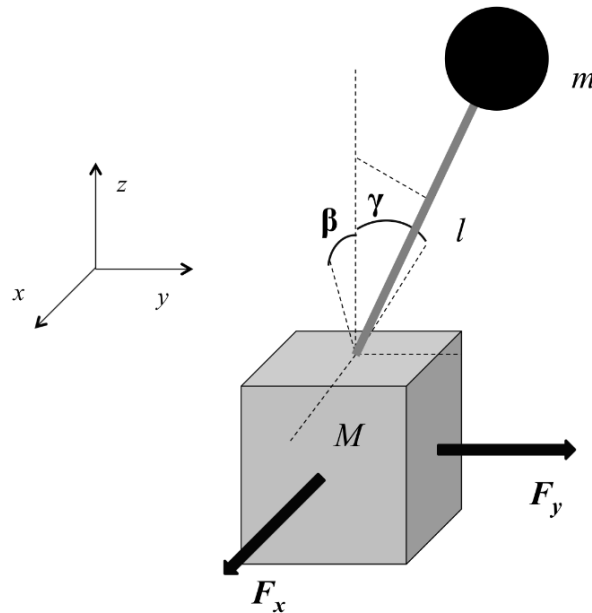


Figure 3.2: Spherical inverted pendulum model in 4 DOF. [3]

If two more degrees of freedom are added, it is more beneficial to use aerial vehicle dynamics notation, Euler angles (yaw, pitch and roll in that order) as seen in Figure 3.3 to describe the attitude of the watercraft, just as the attitude description of an aircraft. [15] The only difference is that the z -axis is pointed upwards as opposed to downwards, as in aircraft notation.

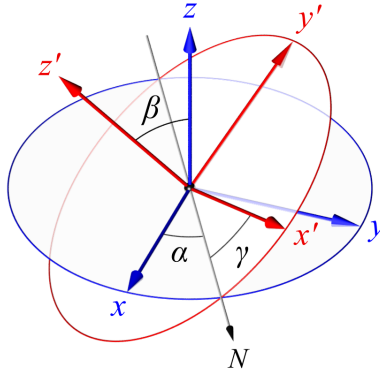


Figure 3.3: Visualization of Euler angles used to describe the orientation of an aircraft. α – Yaw, β – pitch and γ – roll. [4]

In [3], it is concluded from analyzing the controllability matrix, that the system is unreachable when including all six degrees of freedom. The outputs are coupled (i.e. some parameters depend on the same input signal). It is also understood that not all state variables are measured since the number of state variables is reduced to only include the ones that are being measured.

3.1.3 Spherical inverted pendulum model in 5 DOF

The model in Figure 3.4 shows the inverted pendulum on a cart in space with f_x , f_y and f_z as input. This is a good starting point because it has some similarities with the 6 DOF inverted pendulum model of the FoilCart. The reason why it needs to be further extension is that the forces f_x , f_y and f_z are not enough to describe the actuation from the foil. Point B is the position of the hull and given the importance of the hull's orientation, θ needs to be divided into β and γ as in Figure 3.2.

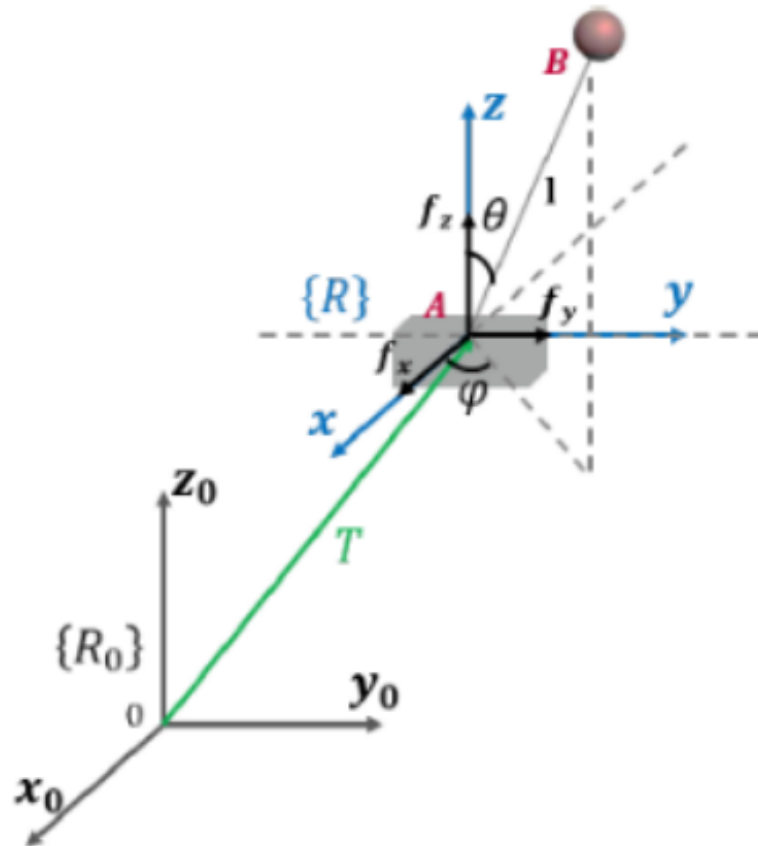


Figure 3.4: 5 DOF model of inverted pendulum or pendulum on a cart in space. [5]

3.1.4 Spherical inverted pendulum model in 6 DOF

To utilize all Euler angles as well as translation in space, the watercraft is modelled with a total of six degrees of freedom.

The extended model is seen in Figure 3.5.

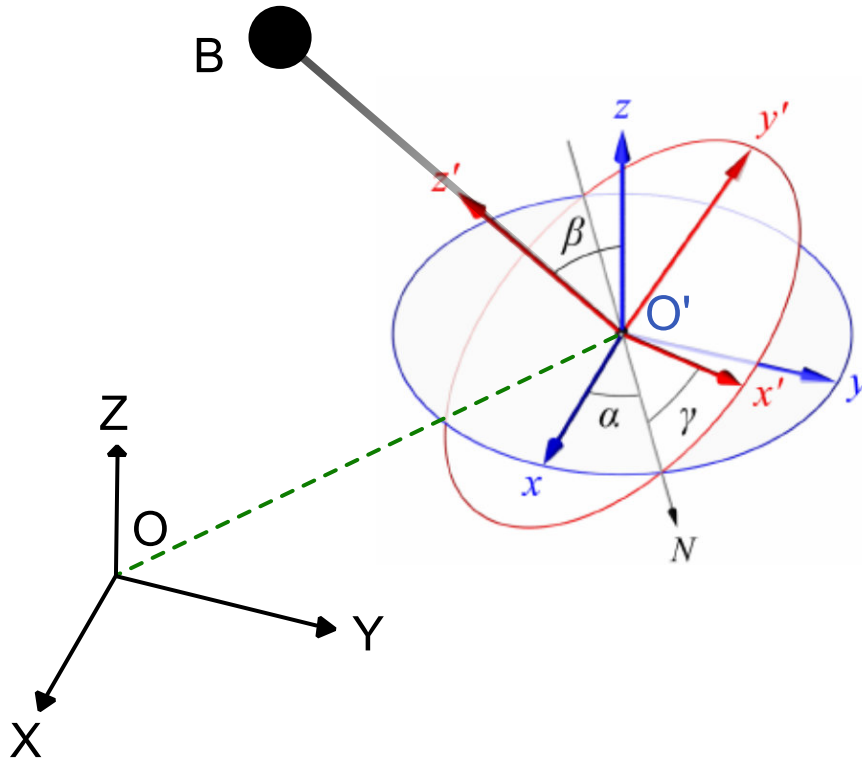


Figure 3.5: The 6 DOF model, using three frames of reference. $OXYZ$ as fixed frame, $O'xyz$ parallel to the fixed frame with origin at the IMU and $O'x'y'z'$ as the IMU coordinate system.

3.2 State space

The state space is a system of differential equations used to describe the dynamics of a system. Since the dynamics are described, the state space needs to include parameters representing all six degrees of freedom as well as their respective derivatives, making it 12 states.

From Figure 3.5, the following parameters can be chosen as state variables to describe

the state in B :

$$z = \begin{bmatrix} z_1 \\ z_2 \\ z_3 \\ z_4 \\ z_5 \\ z_6 \\ z_7 \\ z_8 \\ z_9 \\ z_{10} \\ z_{11} \\ z_{12} \end{bmatrix} \quad (3.1)$$

$$= \begin{bmatrix} X \\ \dot{X} \\ Y \\ \dot{Y} \\ Z \\ \dot{Z} \\ \alpha \\ \dot{\alpha} \\ \beta \\ \dot{\beta} \\ \gamma \\ \dot{\gamma} \end{bmatrix}. \quad (3.2)$$

The system dynamics is then equal to

$$\begin{cases} \dot{z}_1 = z_2 \\ \dot{z}_2 = f_1 \\ \dot{z}_3 = z_4 \\ \dot{z}_4 = f_2 \\ \dot{z}_5 = z_6 \\ \dot{z}_6 = f_3 \\ \dot{z}_7 = z_8 \\ \dot{z}_8 = \tau_\alpha + h_\alpha(z, f) \\ \dot{z}_9 = z_{10} \\ \dot{z}_{10} = \tau_\beta + h_\beta(z, f) \\ \dot{z}_{11} = z_{12} \\ \dot{z}_{12} = \tau_\gamma + h_\gamma(z, f) \end{cases} \quad (3.3)$$

where

$$f = \begin{bmatrix} f_1 \\ f_2 \\ f_3 \end{bmatrix} = g_1(z)u, \quad \text{and} \quad T = \begin{bmatrix} \tau_\alpha \\ \tau_\beta \\ \tau_\gamma \end{bmatrix} = g_2(z)u \quad (3.4)$$

where

$$u = [\delta_1 \quad \delta_2 \quad \delta_3 \quad \delta_4 \quad \delta_5 \quad \delta_6]^T \quad (3.5)$$

are the states of the actuation surfaces, controlled with pulse width modulation (PWM) signals. g_1 and g_2 are nonlinear functions containing formulas for wing dynamics that

give the components of the lift and drag forces as well as torques in O' . h is a nonlinear function that translates forces into torques in O' .

The available sensors are a speedometer which measures speed, an Inertial measurement unit (IMU) [16] that measures angular acceleration and translational acceleration in three directions and two sonars that measure altitude. The states that can be obtained from the measurement data are then speed z_2 and angular accelerations \dot{z}_8 , \dot{z}_{10} and \dot{z}_{12} . The states z_7 , z_9 and z_{11} are angles and can be found by integrating the angular accelerations. The rest need to be estimated.

It is beneficial to choose states using parameters defined in Figure 3.3 as they are compatible with the sensor data from the IMU onboard. The system can then be written on the general form for nonlinear systems:

$$\dot{\mathbf{x}}(t) = f(\mathbf{x}(t), u(t)) \quad (3.6)$$

$$y(t) = h(\mathbf{x}(t)). \quad (3.7)$$

The forces in 3.4 will be computed using the lift and drag equations, (3.8) and (3.9). [17] [18]

$$F_{lift} = \frac{1}{2} \rho v^2 C_L A_{wing} \quad (3.8)$$

$$F_{drag} = \frac{1}{2} \rho v^2 C_D A_{wing}. \quad (3.9)$$

The equations (3.10) and (3.11) for calculating the lift and drag coefficients, are derived in [3] and can be used in this model as well since the same wing is used. As seen below, they only depend on the angle of attack, θ :

$$C_L = -0.0018\theta^2 + 0.003\theta - 0.0314 \quad (3.10)$$

$$C_D = -0.076\theta. \quad (3.11)$$

Chapter 4

Implementation

This chapter presents an implementation of the EKF in Matlab/Simulink. The EKF can be implemented and validated in several ways and here it is implemented in Simulink to make use of an already existing model from a previous thesis work, [3]. Simulink is a software for block diagram environment and is a part of Matlab. It is a convenient way to simulate hardware and is easier to follow than written code.

4.1 Simulink model

The Simulink model inherited from [3] included a plant system and a controller. In Figure 4.1, the plant system is shown as the white box inside the yellow box. It takes actuator deflections as input and returns the the true states, denoted as Perfect States, and the emulated measured states, denoted as Noisy states.

Inputs:

- Wind disturbance forces
- Starboard and port motor thrust forces
- Keel rudder angle
- Elevator angle
- Main wing angle

Outputs:

- Perfect, acutal states
- Noisy, simulated IMU measurement

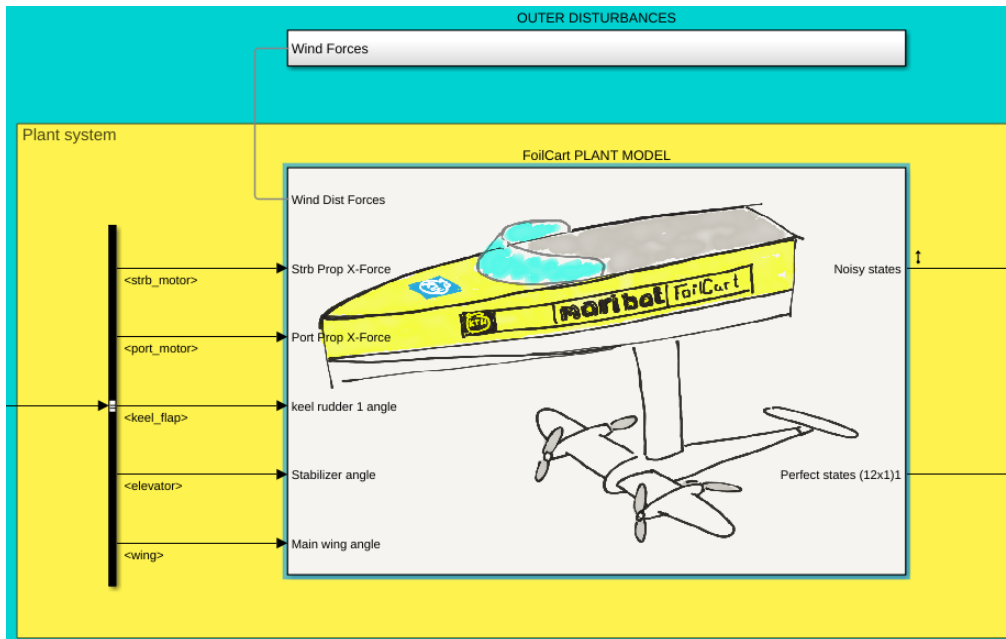


Figure 4.1: Plant system block.

The FoilCart is represented as a spherical inverted pendulum modelled with Simscape Multibody components. Since it is the plant system that is going to be used for validation, the behavior of this block stays unmodified.

In the observer system seen in Figure 4.2, the controller inputs combined with the speed are transformed into forces that are inputs to the system derived in 4.2. Lift and drag equations (3.8) and (3.9) are used to compute the forces from the wings in every timestep. The values of A_{wing} for the different wings are displayed in Table 4.1. Zero order hold blocks are put before the EKF block to simulate delays caused by sampling time.

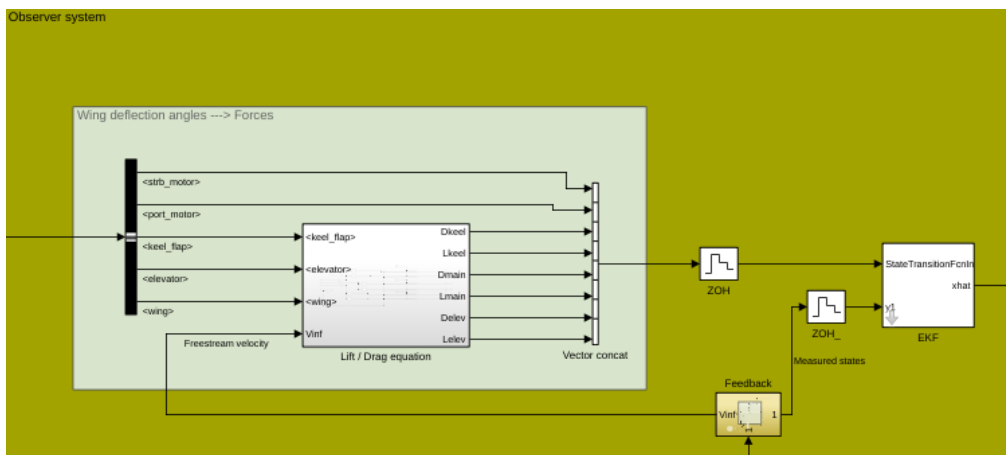


Figure 4.2: Observer system in Simulink.

Figure 4.3 shows how the observer system is connected to the loop without interfering with the system dynamics.

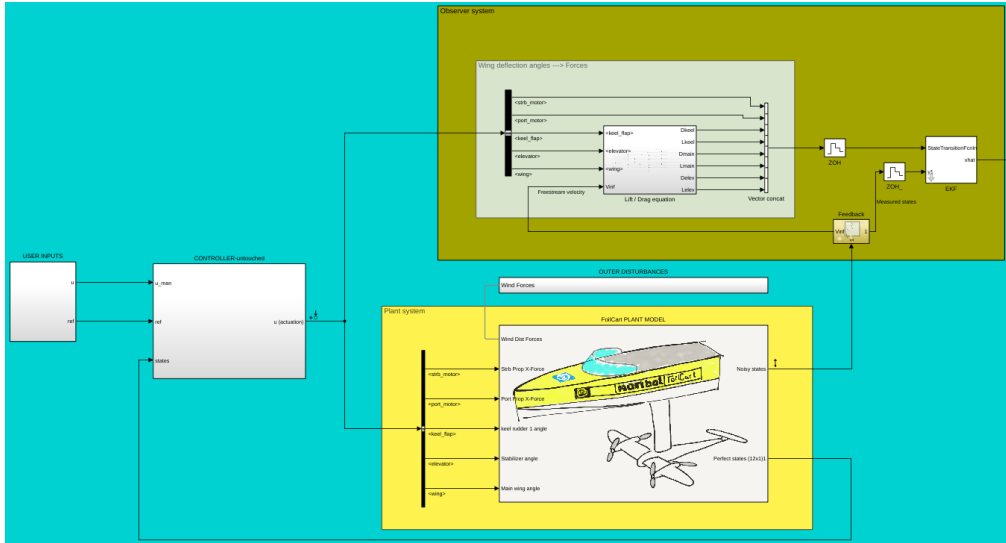


Figure 4.3: Top level view of the Simulink model with observer system attached to the loop.

Table 4.1: Parameters used calculate lift and drag forces in Figure 4.2.

| Parameter | Value |
|----------------------------|-------|
| Area main wing [m^2] | 0.01 |
| Area roll rudder [m^2] | 0.005 |
| Area elevator [m^2] | 0.005 |

To simulate measurement disturbance and make the noisy states noisy, a signal generated by Signal maker is added to the Perfect states. The noise signal can be shaped as white noise and sinusoids or a combination of them both. Since the disturbance is added to the different signals individually, it is possible to customize and mimic the disturbance from real test rides.

The calibration is implemented with a clock. It is not uncommon for micro-controllers to have general purpose timers that can be configured in the same way. If configured properly, a timer does not put any additional load on the CPU.

4.2 Modelling

This section presents the mechanics and mathematical equations used to describe the system dynamics.

4.2.1 Lagrangian mechanics

The spherical inverted pendulum model takes inspiration from the model in Figure 3.4.

In Figure 3.4, the position vectors A and B in the frame R_0 are

$${}^{R_0}A = \begin{bmatrix} x_0 \\ y_0 \\ z_0 \end{bmatrix}, \quad {}^{R_0}B = \begin{bmatrix} x_0 + l \sin \beta \\ y_0 - l \sin \gamma \cos \beta \\ z_0 + l \cos \gamma \cos \beta \end{bmatrix} \quad (4.1)$$

with the velocities

$${}^{R_0}\dot{A} = \begin{bmatrix} \dot{x}_0 \\ \dot{y}_0 \\ \dot{z}_0 \end{bmatrix}, \quad (4.2)$$

$${}^{R_0}\dot{B} = \begin{bmatrix} \dot{x}_0 l \dot{\beta} \cos \beta \\ \dot{y}_0 - \dot{\gamma} l \cos \gamma \cos \beta + \dot{\beta} l \sin \gamma \sin \beta \\ \dot{z}_0 - \dot{\gamma} l \sin \gamma \cos \beta - \dot{\beta} l \cos \gamma \sin \beta \end{bmatrix}. \quad (4.3)$$

The Lagrangian is given by

$$L = T - V, \quad (4.4)$$

where T is the kinetic energy of the system and V is the potential energy of the system. If we recall the definition of kinetic and potential energy

$$\begin{aligned} T = \frac{1}{2} & (m(\dot{x}_0 + \dot{y}_0 + \dot{z}_0 + l\dot{\beta}\cos(x)\cos\beta - l\dot{\gamma}\cos\beta\cos\gamma \\ & - l\dot{\beta}\cos\gamma\sin\beta - l\dot{\gamma}\cos\beta\sin\gamma + l\dot{\beta}\sin\beta\sin\gamma)^2 \\ & + \frac{1}{2}((M+m)(\dot{x}_0^2 + \dot{y}_0^2 + \dot{z}_0^2)) \end{aligned} \quad (4.5)$$

$$V = Mgz_0 + mgl\cos\beta\cos\gamma, \quad (4.6)$$

it will leave us with the following differential equations

$$\frac{d}{dt} \left(\frac{\partial L}{\partial \dot{x}} \right) - \frac{\partial L}{\partial x} = F_x \quad (4.7)$$

$$\frac{d}{dt} \left(\frac{\partial L}{\partial \dot{y}} \right) - \frac{\partial L}{\partial y} = F_y \quad (4.8)$$

$$\frac{d}{dt} \left(\frac{\partial L}{\partial \dot{z}} \right) - \frac{\partial L}{\partial z} = F_z \quad (4.9)$$

$$\frac{d}{dt} \left(\frac{\partial L}{\partial \dot{\alpha}} \right) - \frac{\partial L}{\partial \alpha} = \tau_\alpha \quad (4.10)$$

$$\frac{d}{dt} \left(\frac{\partial L}{\partial \dot{\beta}} \right) - \frac{\partial L}{\partial \beta} = \tau_\beta \quad (4.11)$$

$$\frac{d}{dt} \left(\frac{\partial L}{\partial \dot{\gamma}} \right) - \frac{\partial L}{\partial \gamma} = \tau_\gamma. \quad (4.12)$$

As predicted by Strömqvist after deriving the 4 DOF equations of motion in [3], the equations of motion (4.7) - (4.12) will have high algebraic complexity.

"There is no understatement to say that the dynamics complexity increases heavily by introducing two more degrees of freedom in terms of movement, which further suggests that to mathematically model all six degrees would be an enormous task. Not only are the expressions longer but also highly non-linear, adding further difficulties to design control algorithms."[3]

4.2.2 Newtonian mechanics

To minimize the risk of errors, the use of Newtonian mechanics is an more attractive alternative. It is derived by computing the impact of one input force at a time.

To make use of the sensor data from the IMU, the orientation of the vessel is described by the following rotation matrix,

$$T_{yaw} = \begin{bmatrix} \cos \alpha & -\sin \alpha & 0 \\ \sin \alpha & \cos \alpha & 0 \\ 0 & 0 & 1 \end{bmatrix} \quad (4.13)$$

$$T_{pitch} = \begin{bmatrix} \cos \beta & 0 & \sin \beta \\ 0 & 1 & 0 \\ -\sin \beta & 0 & \cos \beta \end{bmatrix} \quad (4.14)$$

$$T_{roll} = \begin{bmatrix} 1 & 0 & 0 \\ 0 & \cos \gamma & -\sin \gamma \\ 0 & \sin \gamma & \cos \gamma \end{bmatrix} \quad (4.15)$$

$$T_{rot} = T_{yaw}T_{pitch}T_{roll}. \quad (4.16)$$

The input forces are defined as shown in Figure 4.4.

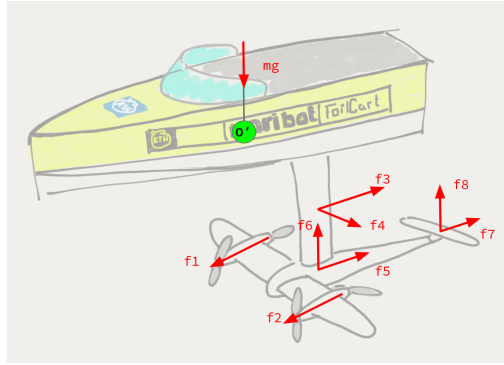


Figure 4.4: Input modelling.

The lengths in Figure 4.4 are defined by the dimensions shown in Figure 4.5.

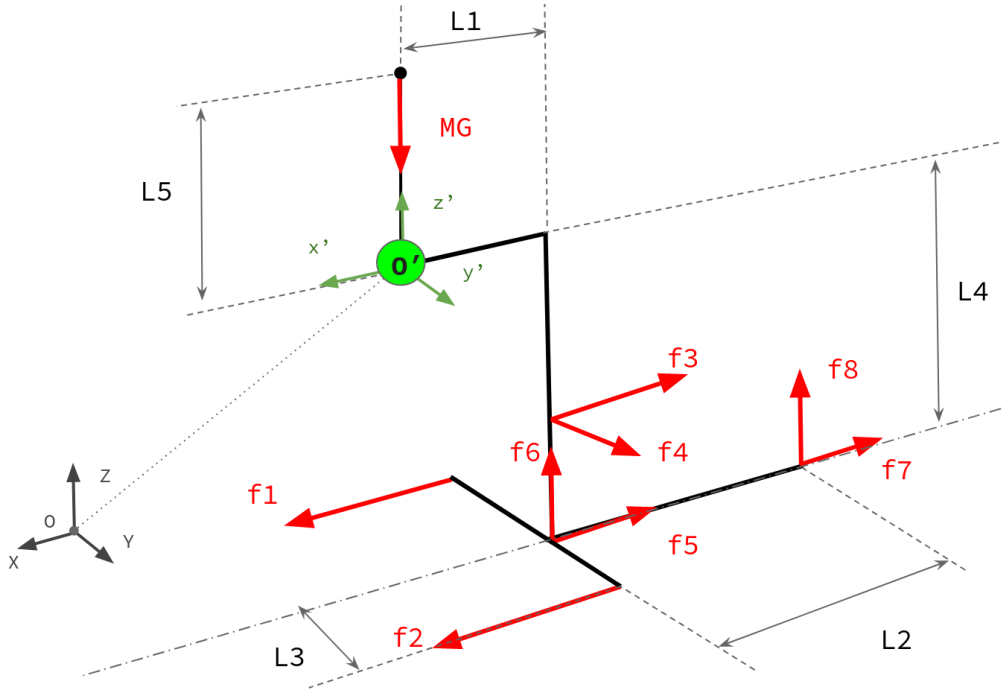


Figure 4.5: Dimensions of input modelling.

The parameters for Figure 4.4 - 4.5 are shown in Table 4.2.

Table 4.2: Parameters used to derive the 6 DOF model.

| Parameter | Real | Scaled |
|--|--------|---------|
| Mass, M [kg] | 150.85 | 150.85 |
| Moment of inertia, I_{xx} [kgm^2] | 3.9 | 3.9 |
| Moment of inertia, I_{yy} [kgm^2] | 20.5 | 20.5 |
| Moment of inertia, I_{zz} [kgm^2] | 20.0 | 20.0 |
| Gravity constant, G [ms^{-2}] | 9.82 | 9.82 |
| Sampling time, H [s] | 0.005 | 0.005 |
| $L1$ [m] | 0.50 | 0.00005 |
| $L2$ [m] | 0.40 | 0.00004 |
| $L3$ [m] | 0.65 | 0.00007 |
| $L4$ [m] | 1.0 | 0.0001 |
| $L5$ [m] | 1.0 | 0.0001 |

Recalling the definition of torque:

$$\tau = r \times F. \quad (4.17)$$

Hence, the torque τ in the point O' in Figure 4.5 for each force can be obtained by finding the the cross-product as in (4.17) where r is the lever arm vector from O' to the point where force F is applied.

Using this method, the torques caused by the different input forces in Figure 4.5 are displayed in (4.18) - (4.24).

Motors

$$\tau_{motor,starboard} = [-L1, L3, -L4] \times [f_1, 0, 0] \quad (4.18)$$

$$\tau_{motor,port} = [-L1, -L3, -L4] \times [f_2, 0, 0] \quad (4.19)$$

Keel rudder

$$\tau_{keel} = [-L1, -L3, -L4] \times [-f_3, f_4, 0] \quad (4.20)$$

Main wing

$$\tau_{main} = [-L1, 0, -L4] \times [-f_5, 0, f_6] \quad (4.21)$$

Elevator

$$\tau_{elevator} = [-(L1 + L2), 0, -L4] \times [-f_7, 0, f_8] \quad (4.22)$$

Gravity

$$\tau_{gravity} = [0, 0, L5] \times [(MG \sin z_{11} \cos z_9), (MG \sin z_9 \cos z_{11}), 0] \quad (4.23)$$

Total torque

$$\tau_{tot} = \sum_i \tau_i. \quad i \in \{motor, starboard; motor, port; keel; main; elevator; gravity\} \quad (4.24)$$

Total force

The total force is obtained by summarizing all forces in Figure 4.5 along the axes x' , y' and z' respectively. The forces are then rotated using the rotation matrix (4.16) since $O'x'y'z'$ is the coordinate system of the IMU, which is fixed to the orientation of the FoilCart. Therefore, the gravitational force is not transformed since it is always pointing in negative Z direction in the frame $OXYZ$ in Figure 4.5.

Using this method results in the following expression (4.25) for the force.

$$F_{tot} = T_{rot} [(f_1 + f_2 - f_3 - f_5 - f_7), f_4, (f_6 + f_8)] + [0, 0, -MG] \quad (4.25)$$

Equations of motion

Recalling Newton's second law, also known as *Force equals mass times acceleration* (4.26). The corresponding equation for torque is *moment of inertia times angular acceleration* (4.27).

$$F = ma \quad (4.26)$$

$$\tau = I\ddot{\theta}. \quad (4.27)$$

Given the mass and moment of inertia from Table 4.2 used in (4.26) and (4.27), the equations of motion are then

$$\dot{\mathbf{z}} = \begin{bmatrix} z_2 \\ F_{tot}[0]/M \\ z_4 \\ F_{tot}[1]/M \\ z_6 \\ F_{tot}[2]/M \\ z_8 \\ \tau_{tot}[0]/I_{zz} \\ z_{10} \\ \tau_{tot}[1]/I_{yy} \\ z_{12} \\ \tau_{tot}[2]/I_{xx} \end{bmatrix}. \quad (4.28)$$

As mentioned before, the controller is digital and lives in the discrete-time space. Therefore it is a good idea to express the equations of motion as equations of difference rather than differential equations, as shown below:

$$z[t_k + kh] = A_d z[t_k] + B_d u[t_k + kh]. \quad (4.29)$$

To discretize (4.28), linear approximations of the system are obtained by the Jacobians, as shown below:

$$A_c = \frac{\partial}{\partial \mathbf{z}} \dot{\mathbf{z}} \quad (4.30)$$

$$B_c = \frac{\partial}{\partial u} \dot{\mathbf{z}} \quad (4.31)$$

where $u = [f_1 \quad f_2 \quad f_3 \quad f_4 \quad f_5 \quad f_6 \quad f_7 \quad f_8]$ and

$$A_d = e^{A_c h} \quad (4.32)$$

$$B_d = \int_{s=0}^h e^{A_c s} B_c ds. \quad (4.33)$$

$e^{A_c h}$ is the matrix exponential of A_c with sampling time h . To make it easier to implement on a microcontroller, a power series can be used as approximation of the matrix exponential, as shown below:

$$\begin{aligned} e^{A_c H} \approx & I_{12} + H A_c + (H H / 2)(A_c A_c) + (H H H / 6)(A_c A_c A_c) \\ & + (H H H H / 24)(A_c A_c A_c A_c). \end{aligned} \quad (4.34)$$

Since the sampling time $H = 0.005$ s and $H^4 = 6.25 \cdot 10^{-10}$, additional terms that are added to the power series will be small enough to be approximated as zero. Matrices A_d and B_d using (??) can be seen in Appendix A, in Matlab notation.

4.3 Extended Kalman Filter

The Kalman filter is constructed by using the model derived in previous chapter as model in the observer system. Initially, the tuning parameters Q_k and R_k are both set to identity matrices. The intuition behind that is that the model input and the measured states are weighted equal when computing the observer states. The initial observer gain can then be adjusted by changing the values of Q_k and R_k . If Q_k is low compared to R_k , more trust is put on the model over the measurements.

4.4 Sensor fusion

Sensor fusion is the process of combining sensor data from different sources to reduce uncertainty in the variable that is measured. State estimation can be used to reduce the number of sensors required in a system. Sensor fusion has the opposite effect since it increases the number of sensors without providing additional states. In this case, the purpose is to increase the accuracy of the altitude measurement by using data from two sonars and one IMU.

In order to include altitude as a degree of freedom, the altitude needs to be measured. The current measurement of the altitude can be seen in Figure 4.6. It is seen that the altitude data oscillates, even when the speed is 0 kts. This is due to waves on the surface. Using this data as baseline when controlling the altitude would be uncomfortable for passengers on board, in a similar way as when riding a car without suspension on a rocky road. The purpose of using an EKF together with sensor fusion is to define the baseline as a plane where the water surface would be if there was no waves. Then, the FoilCart would ride through the waves instead of on the waves.

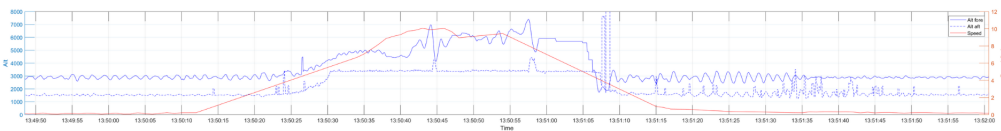


Figure 4.6: Altitude data from a test ride with the full scale prototype. The blue lines are altitude data from sonars in the aft and the fore. The red line is speed.

The IMU used in the FoilCart is a STIM300 [16], which is an accelerometer and a gyroscope. It measures angular acceleration and translational acceleration. The angles and positions are obtained through integration. Since the integration is done numerically, there is an integration error that accumulates over time, called drifting. To avoid drifting and get more accurate measurements of the altitude, additional data from sonars can be used. The sonars are not prone to drifting and are more reliable than the IMU to measure altitude. The sonars are only sampled with a frequency of 2 Hz instead of 200 Hz as the IMU. This means that the altitude measurement can be calibrated every 0.5 seconds to avoid drifting and the IMU only has to integrate for 100 timesteps at a time.

The altitude is estimated by combining the sensor data from the two sonars with the Euler angles. First, the altitude for each sonar is computed by using trigonometry for a right-angled triangle, as in (4.35). Then, the altitude of the IMU is estimated as the mean of the altitude in the fore and the altitude in the aft.

Assuming the setup shown in Figure 4.7, the distance from the sonar to the water is obtained by combining data from sonar with data from the IMU. Given the pitch β and the roll γ , the altitude of the sonar is calculated as follows:

$$d = r \cos \beta \cos \gamma. \quad (4.35)$$

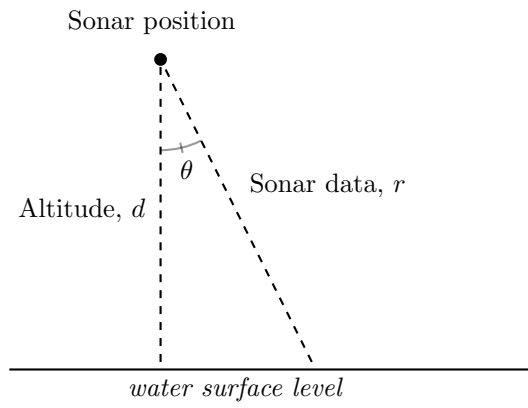


Figure 4.7: Two dimensional trigonometry for calculating the altitude using sensor fusion. θ is the angle between the axis perpendicular to Earth and the IMU's z-axis.

Chapter 5

Results

For a systematical validation of the model, there are three different outputs to consider:

- The output from the simulink model which is considered as *perfect* output;
- Distorted output from the simulink model to mimic measured states from the IMU;
- The output from the observer, the estimated states.

The main focus when analysing the results is to see how well the estimated states matches with the perfect states.

5.1 Pitch case

In this first case, the FoilCart starts with an initial velocity of around 4 kts and accelerates up to 8 kts. This case should not affect the yaw or roll because the absence of lateral forces. To validate those degrees of freedom, a different case has to be used.

5.1.1 Perfect states

It is seen in Figure 5.1, the controller is driving the system to a steady state. When validating the observer system, the controller performance is irrelevant. The first step is to only attach the observer system to the loop and tune it so that it produces estimates that are reasonably close to the perfect states. The results in Figure 5.1 is considered as the benchmark when evaluating EKF performance in the pitch case.

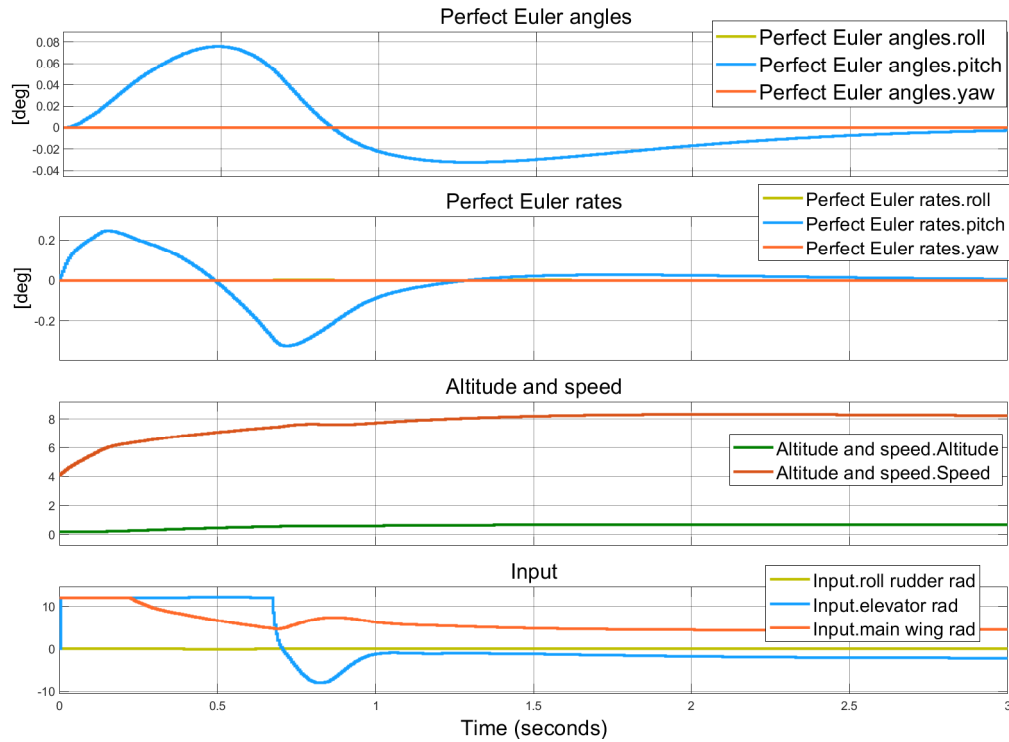


Figure 5.1: Simulation output considered as perfect states, unaffected by disturbances.

5.1.2 Estimated states

Figure 5.2 shows the EKF output based on the model derived in 4.2.2 together with the perfect output from Figure 5.1. It is noticeable that the two outputs differ since the EKF output does not align with its corresponding perfect output.

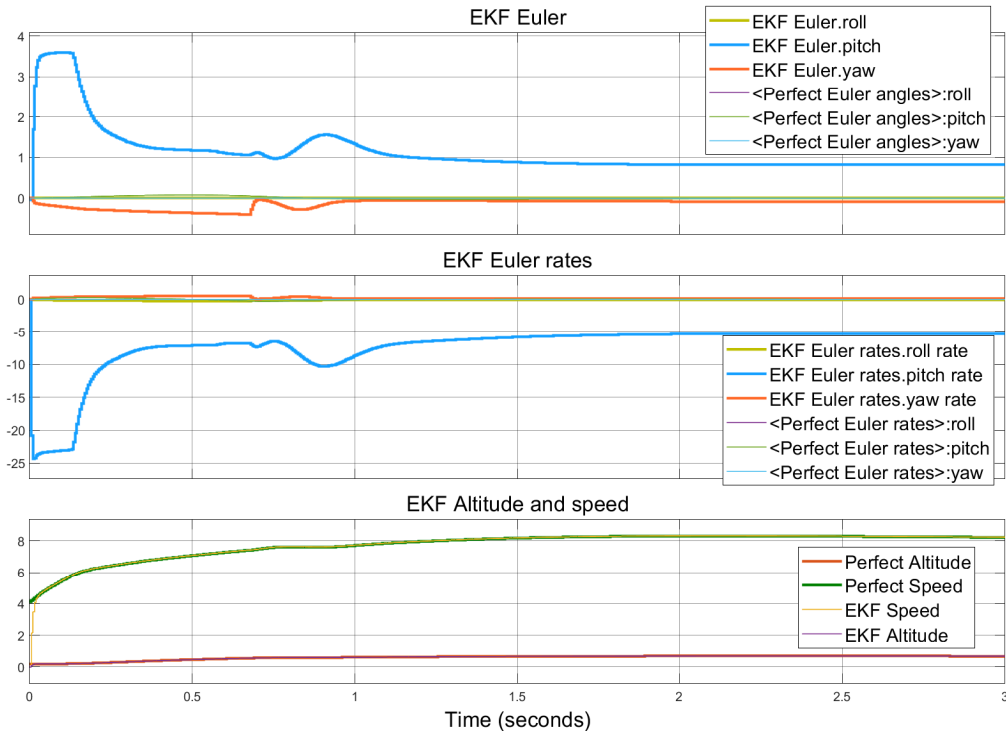


Figure 5.2: Observer states with no disturbance

This is not the result that we wanted, but it is the result that we got. It is not necessarily the mechanics that is wrong, even if the result provides very little evidence that it is correct. In the next paragraph, the absence of fluid mechanic components in the model is discussed as a possible source of error.

5.1.3 Scaling the dimensions to slow down system dynamics in observer system

As also mentioned in [3], the FoilCart in the Simulink model is represented as a damped spherical inverted pendulum to simulate the water resistance. The spherical inverted pendulum model in the observer system is undamped and assumes no forces from a surrounding medium except the lift and drag forces on the wing surfaces.

One way to mimic the behavior of forces from a surrounding medium is to reduce the impact of input forces. From (4.17), it is concluded that decreasing either the force F or length of the lever arm vector r will result in lower torque τ .

If $F_A = F_B$ in Figure 5.3, F_A would cause weaker torque on the red dot than F_B .

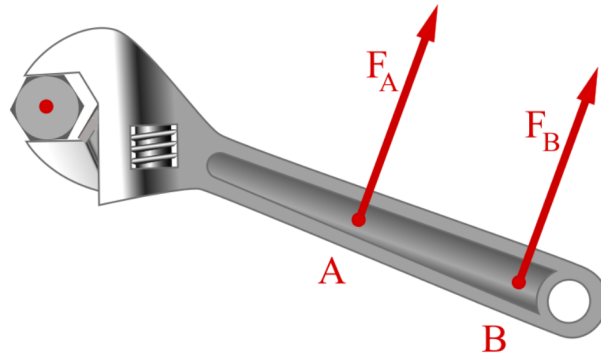


Figure 5.3: A wrench that shows how the torque in the red dot can be changed by modifying the distance from the red dot to the point of force application, (r in (4.17)).

The result of shortening the length of the lever arm vector with a factor 0.0001, referred to as the Scaled parameters in Table 4.2, is shown in Figure 5.4. It is seen that the EKF Euler graph starts to align with the perfect output around the 1.0 second mark.

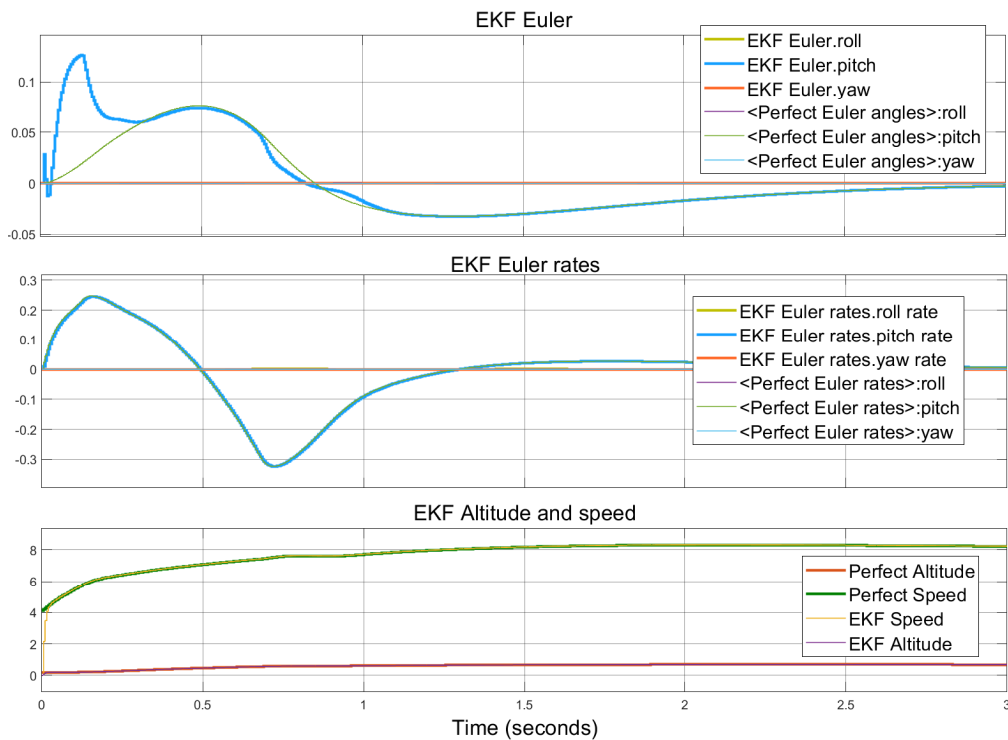


Figure 5.4: Observer states with no disturbance. Dimensions scaled by a factor 1/1000.

5.1.4 Tuning the EKF

In order to make the EKF converge faster, the observer gain needs to converge to the near-optimal Kalman gain faster. Figure 5.5 shows the result of increasing the process noise covariance $Q_k = 2I_{12}$. It is seen that the EKF Euler graph converges faster than in Figure 5.4 and that the overshoot around 0 seconds is smaller.

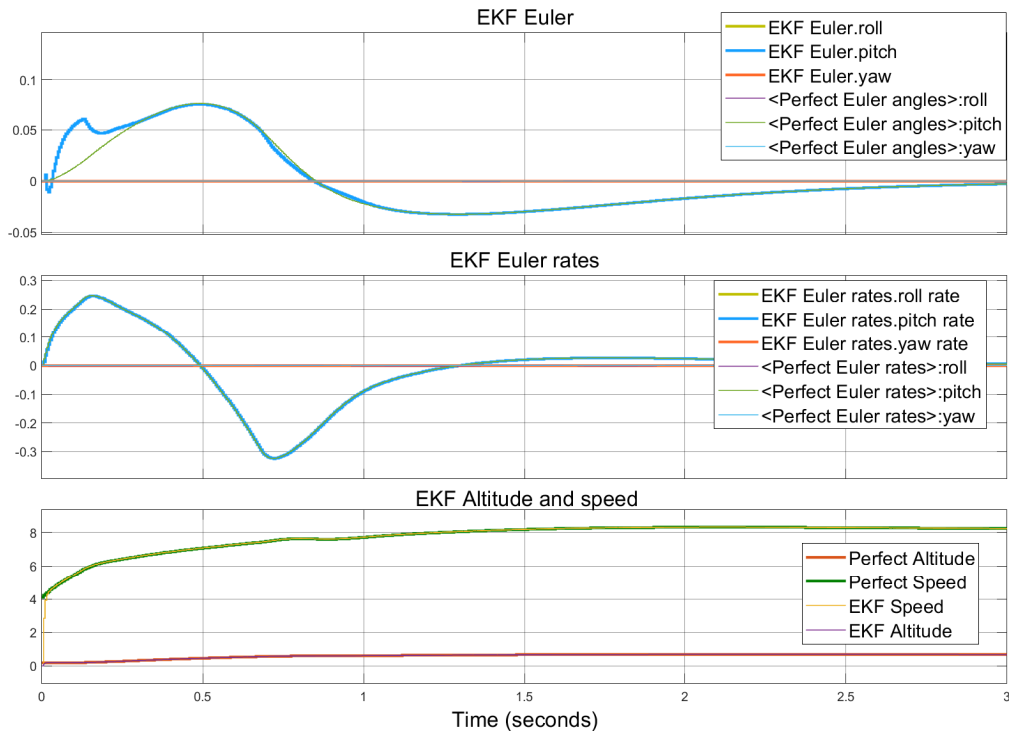


Figure 5.5: Observer states with no disturbance. EKF tuned with $Q_k = 2I_{12}$ and $R_k = I_{12}$ to put more weight on the measured output rather than the output from the model.

5.1.5 Sinusoidal disturbance

To investigate the robustness of the EKF, measurement disturbance is emulated in the IMU output. To not interfere with the system dynamics, the perfect states are used as feedback to the controller.

The disturbance was added with the Signal creator in Simulink. Figure 5.6 shows the simulated measured output with a sinusoidal disturbance. There are two sensor outputs for the altitude, one in the fore and one in the aft. The data from the sonars is sampled with a frequency of 2 Hz.

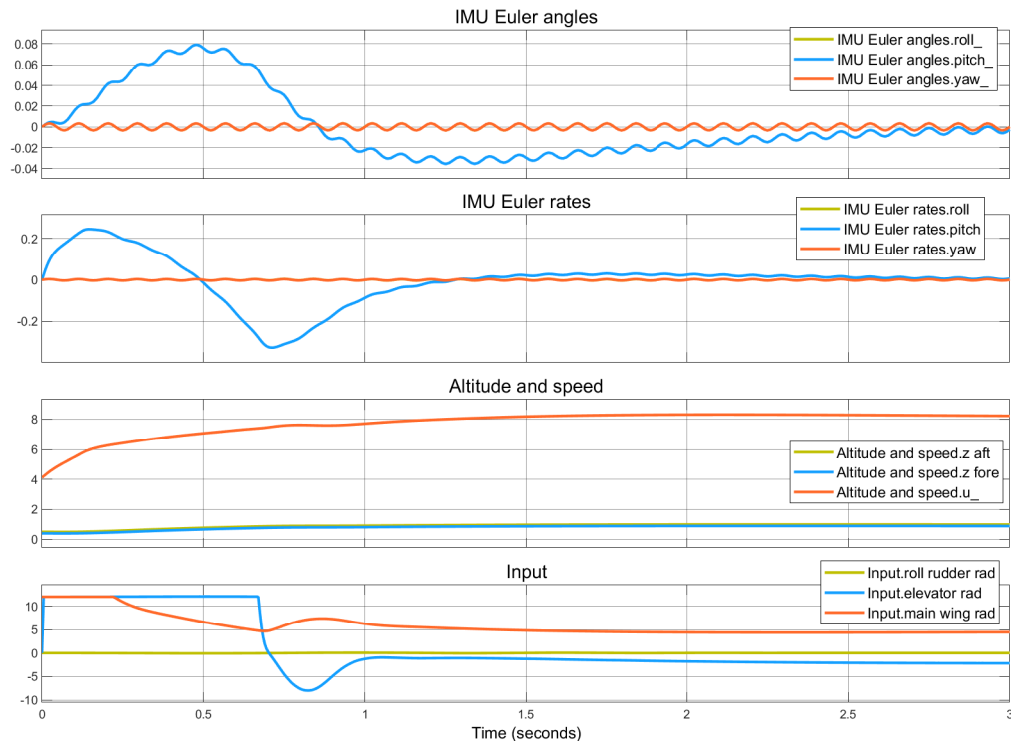


Figure 5.6: Measurement with sinusoidal disturbance.

In Figure 5.7, it is seen that the output from the EKF converges even in the presence of sinusoidal disturbance.

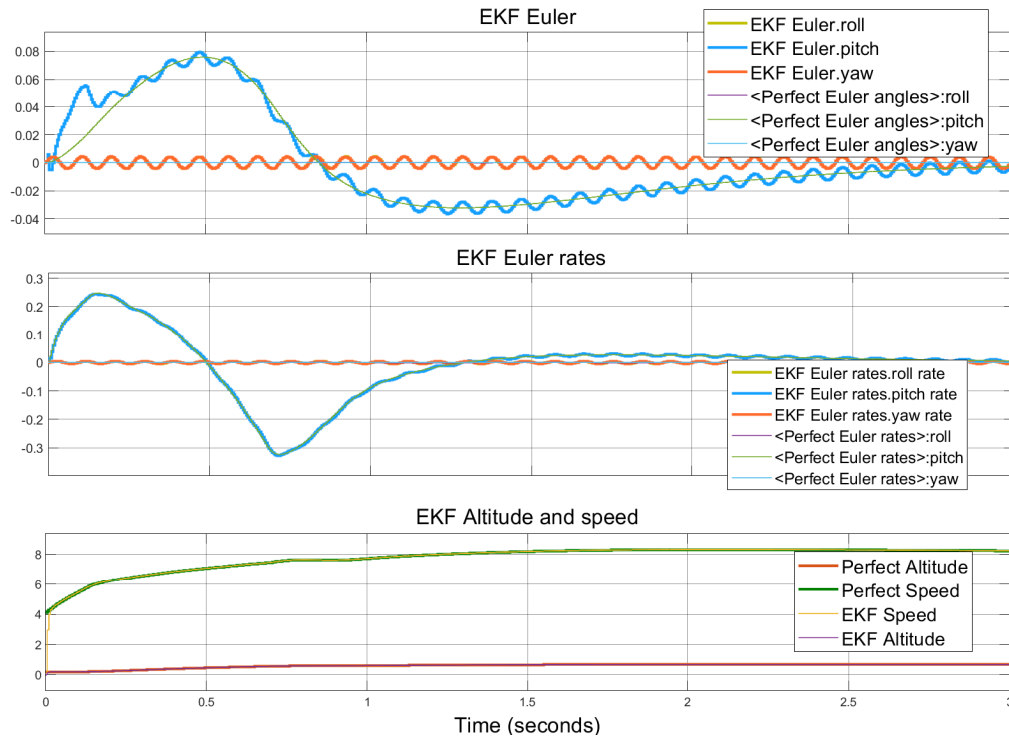


Figure 5.7: Observer states with sinusoidal disturbance.

5.1.6 Lowpass-filter

It is possible to get rid of some of the oscillations with a lowpass-filter, as seen in Figure 5.8. A side effect of removing the oscillations with a lowpass-filter is that the system takes longer time to converge. The lowpass-filter will also increase the load on the CPU. This is enough reason to not use a lowpass-filter after the EKF.

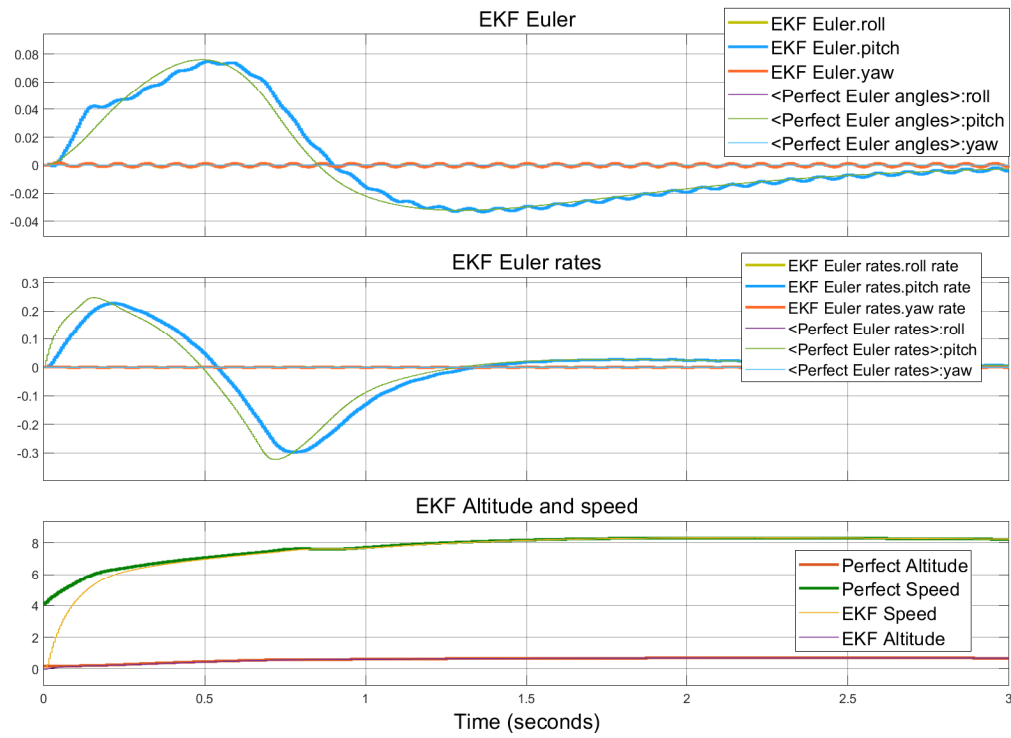


Figure 5.8: Lowpass-filtered observer states with sinusoidal disturbance.

5.1.7 White noise disturbance

Figure 5.9 shows the effects of adding white noise as disturbance to the measured output.

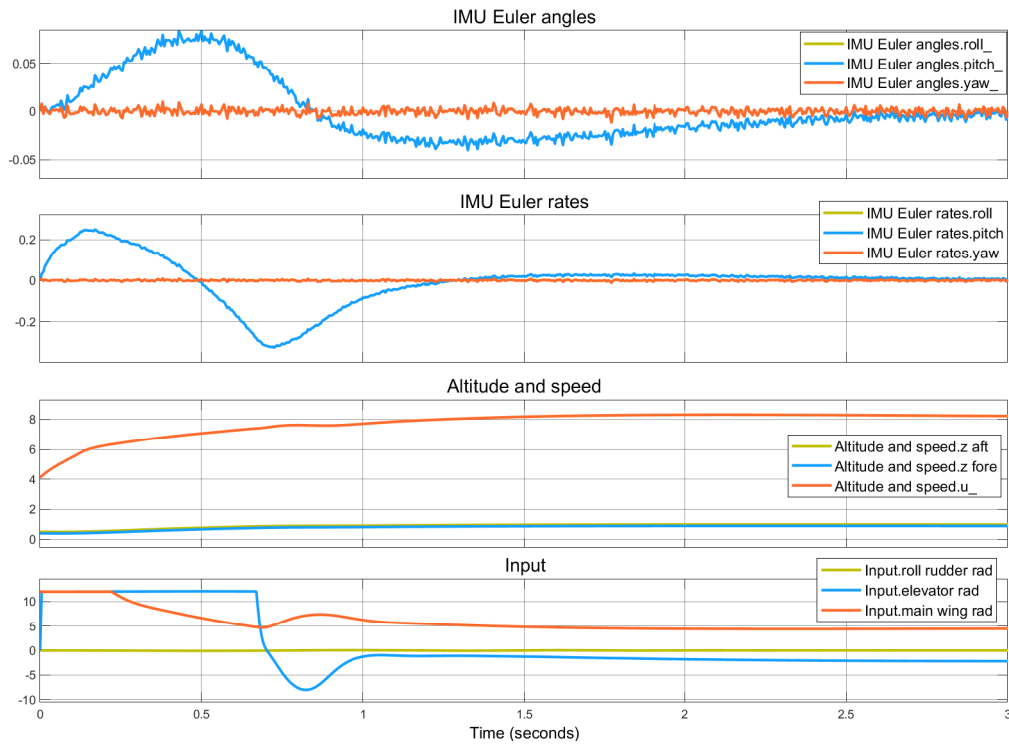


Figure 5.9: Measurement with white noise disturbance.

In Figure 5.10, it is seen that the EKF Euler output aligns with the perfect output at around 1.2 seconds. This is because the covariance estimate (2.10) has converged to the near-optimal value. Once the observer system has converged, it is shown to give a more accurate estimation of the perfect states than the measured output in Figure 5.9.

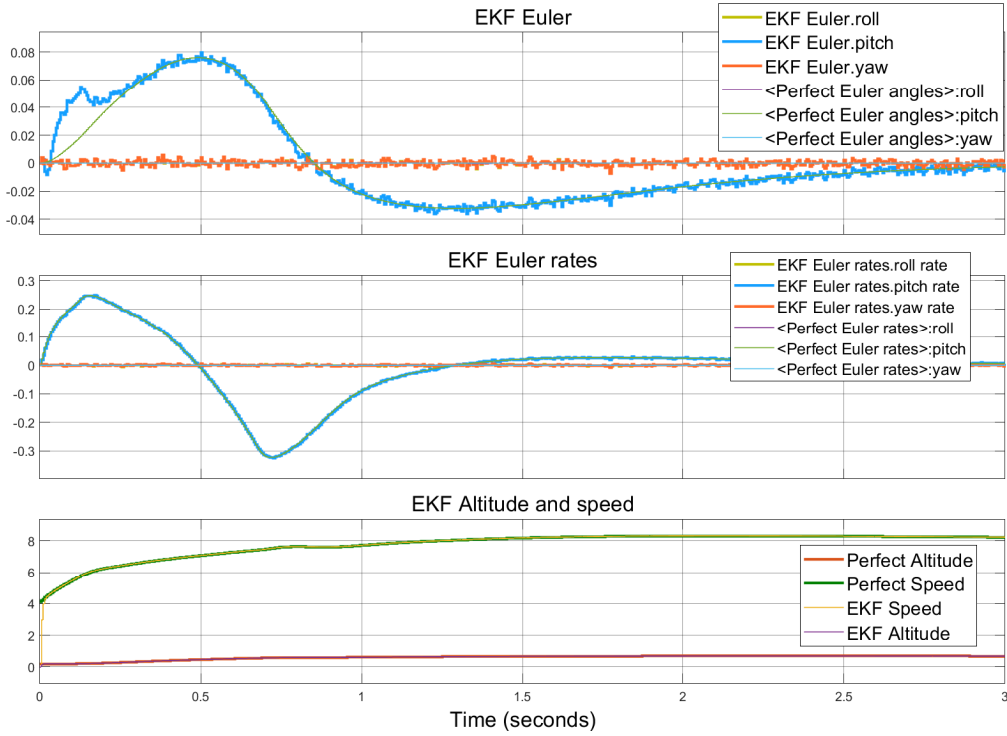


Figure 5.10: EKF output in presence of white noise disturbance with tuning parameters $Q = 8I_{12}$ and $R = 7I_{12}$.

From the results above, it can be concluded that the EKF works as intended for the pitch parameter in terms of providing an accurate estimate of the perfect output. To make the estimate converge faster, the initial values of P_k matrix should be chosen such that the initial Kalman gain (2.8) becomes higher. It can also be done by increasing the measurement noise covariance Q compared to the process noise covariance R . Then more trust is put on measurements rather than on the prediction. If the measurements are given too much trust over the prediction, the prediction will not remove any stochastic noise from the estimate.

5.1.8 Altitude estimation

By looking at Figure 5.11, it is seen that the EKF gives an accurate estimation of the true altitude. A reason that the estimates are that accurate may be that the exact position of the sonars is known so that simulated offsets have no effect since they are transformed back immediately. The altitude estimation is also more accurate than the pitch estimation. It can then be concluded that the complexity of modelling translation is lower than the complexity of modelling rotation.

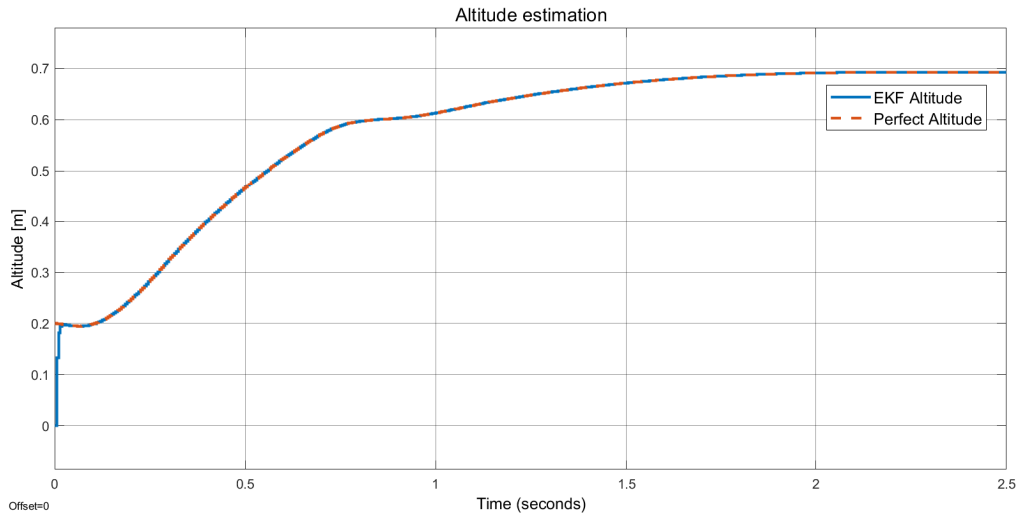


Figure 5.11: Estimation of the altitude with EKF.

In Figure 5.12, it is seen that the EKF is robust and can give an accurate estimation of the altitude with simulated white noise in the simulated measurement. This is disturbance only in the measurement and not on the water surface. However, if a plane is considered as the baseline, then small waves can be treated as measurement noise. The Measured Altitude in Figure 5.12 is the mean of the fore sonar altitude and aft sonar altitude.

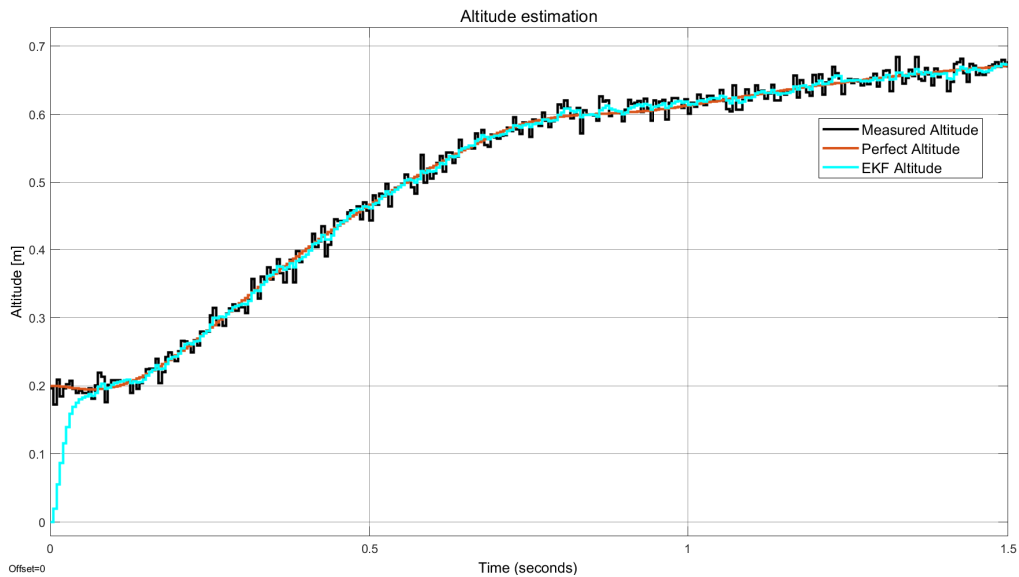


Figure 5.12: Altitude estimation with EKF parameters $Q = I_{12}$ and $R = 8I_{12}$ in the presence of white noise disturbance.

5.2 Roll case

In the roll case, the FoilCart starts in a flying state at 8 kts with and a roll angle of 0.1 degrees. No measurement noise is added in this case.

5.2.1 Perfect states

It is seen in Figure 5.13 that roll error is corrected and that the system is driven to a steady state.

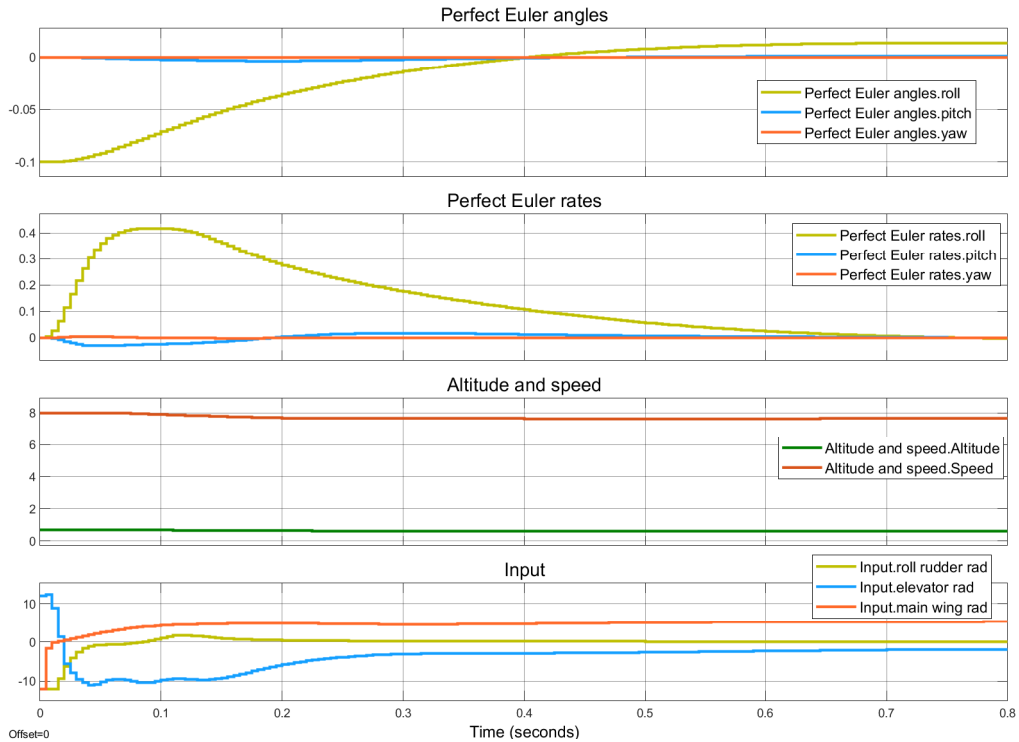


Figure 5.13: Perfect states for roll case without disturbance.

5.2.2 Estimated states

The output from the EKF can be seen in Figure 5.14. In the first graph in Figure 5.14, it is seen that the observer system is very responsive to the control input, seen in the bottom graph in Figure 5.13. This causes an overshoot for the pitch and yaw estimates but is still able to converge.

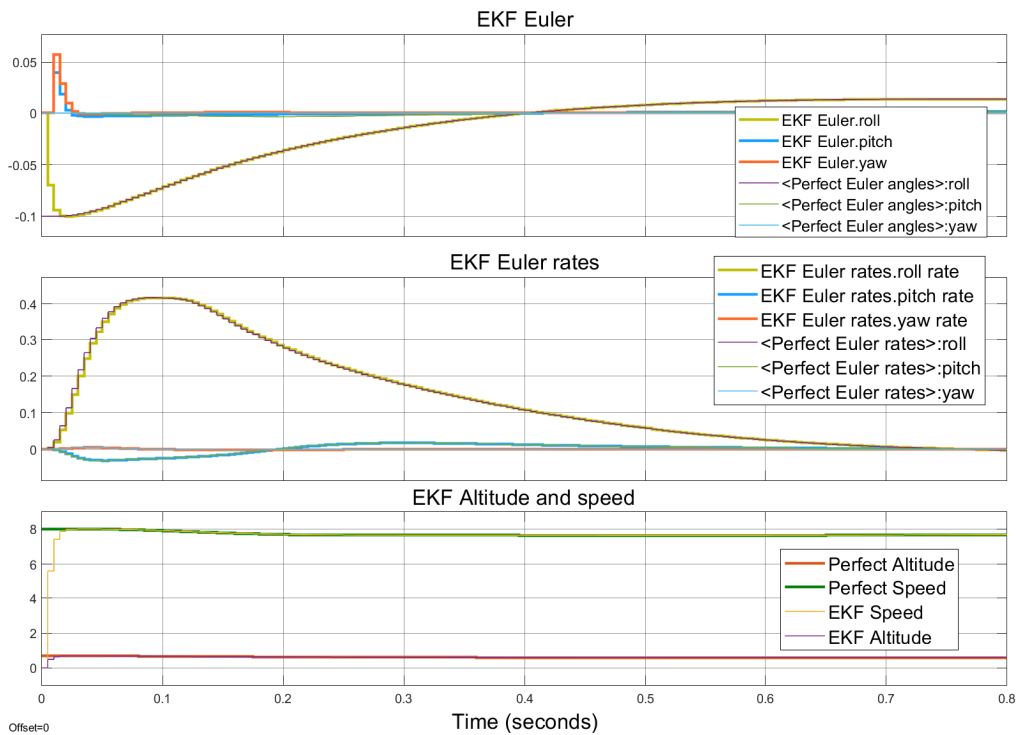


Figure 5.14: Observer states for roll case without disturbance.

5.3 Yaw case

In the yaw case, the FoilCart starts in a flying state at 8 kts and with a yaw angle of 0.1 degrees. No measurement noise is added in this case.

5.3.1 Perfect states

In Figure 5.15, it is seen that the yaw error is corrected and that the system is driven to a steady state.

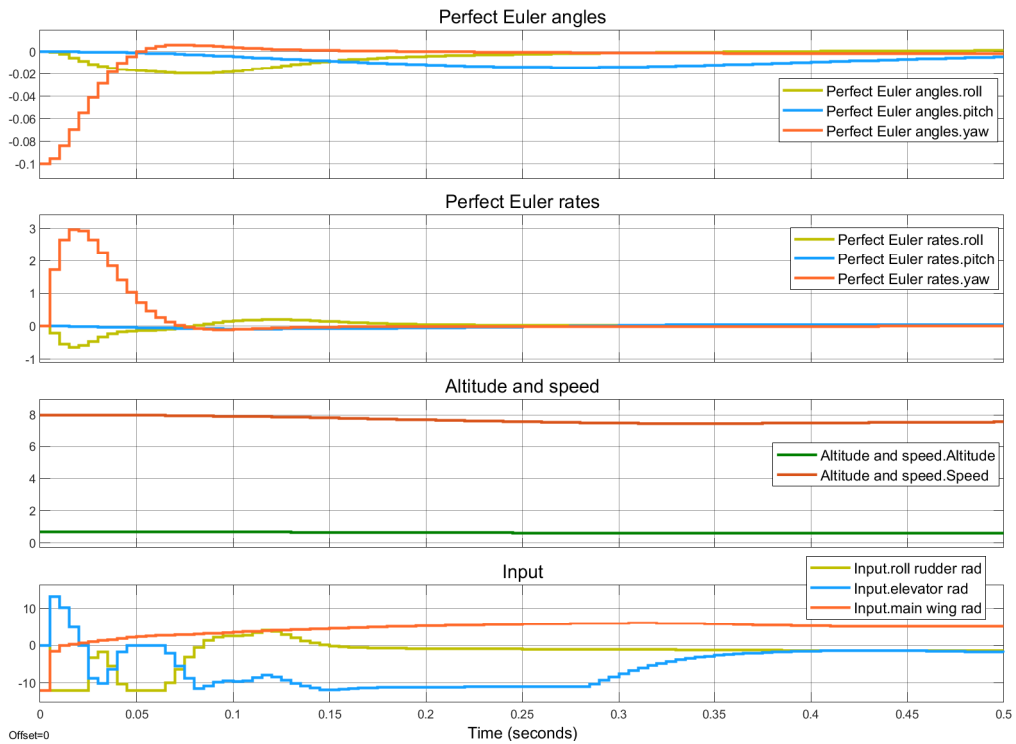


Figure 5.15: Perfect states for yaw case without disturbance.

5.3.2 Estimated states

Figure 5.16 shows the EKF output. As in the roll case, the observer system is very responsive to the control input. Pitch and yaw estimates have an overshoot but is able to provide accurate state estimation once converged.

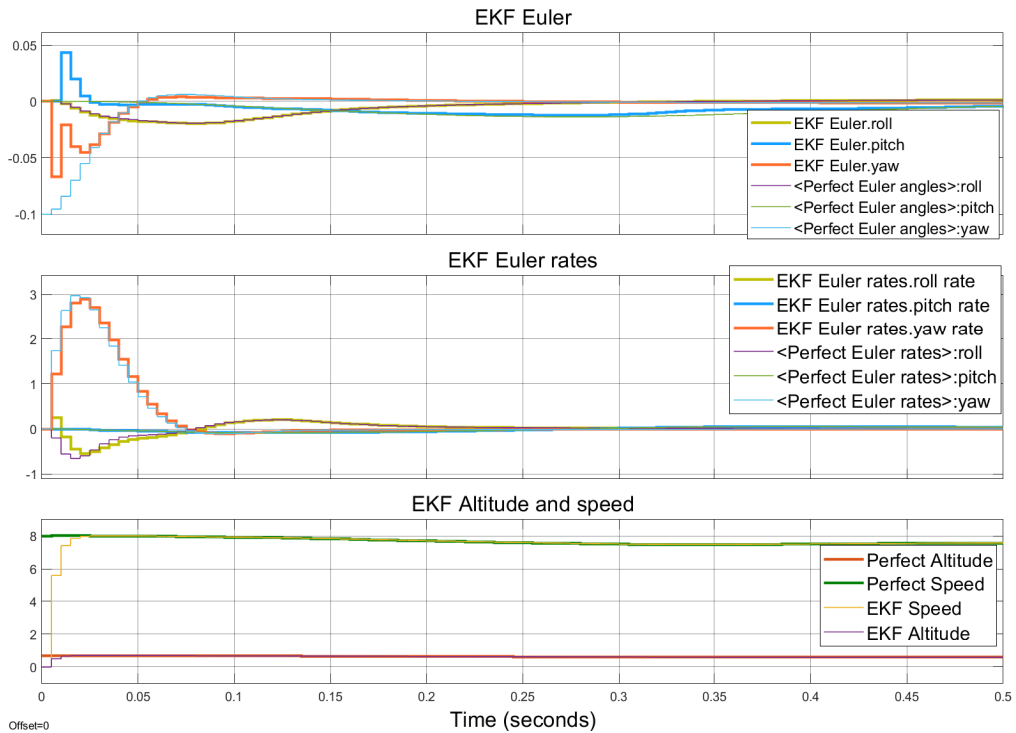


Figure 5.16: Observer states for yaw case without disturbance.

5.4 Discussion

Since a model of the FoilCart was used to validate another model of the FoilCart, the accuracy of the model derived in this thesis comes with some degree of uncertainty. Even if the Simulink model does not replicate every single aspect of the real prototype, it still be used to validate those aspects that it can replicate. For example, Simulink Multibody and Aerospace Toolbox are tools for mechanical simulations. Dynamics of fluids, like water, are therefore heavily simplified.

Despite that, the results pointed to that this could be a candidate for replacing the existing 4 DOF model in [3] due to the two additional degrees of freedom, altitude and yaw.

Chapter 6

Conclusion and Future Work

This chapter aims to give a summary of the results of this thesis and to answer the research question from the Introduction chapter. The conclusion is followed by a future work-section where suggestions on how the same topic can be further investigated by using other methods that are not used in this thesis.

6.1 Conclusion

The question whether a hydrofoiling watercraft with super compact hydrofoiling module can be modelled as an inverted pendulum has led to some interesting conclusions. The results in Chapter 5 show that a hydrofoiling watercraft with super compact hydrofoiling module can be modelled as an inverted pendulum. The inverted pendulum model in combination with an Extended Kalman Filter also makes it useful for state estimation when stochastic noise is present, like for example measurement noise and irregularities on the water surface. It is also concluded that advanced fluid dynamics are left for future work due to lack of expertise and software.

This thesis presents a derivation of how the FoilCart could be modelled as a spherical inverted pendulum using Newtonian mechanics. The model is derived without linearizing or simplifying trigonometric expressions. To contain input-output couplings in the system dynamics, the system is not divided through superposition. This also opens up for altitude control and yaw control, which are not compatible with the 4 DOF model.

The model is derived from the mechanical dynamics. It should however be considered in the future to investigate if including viscous effects from the surrounding water in the model could increase the performance of the observer. Within the scope of this thesis, mechanics can only take us this far.

Since EKF is the choice of state estimator, linearization of the system dynamics is inevitable. The EKF is a well known and widely used method in nonlinear state estimation but since it is a linearizing method, it cannot be seen as optimal and it is only locally stable. A reasonably good initial guess \hat{x}_0 and/or weak nonlinearities in the system are required in order for the Kalman gain to converge to a near-optimal value. Otherwise, the estimates will show divergent behavior.

6.2 Future work

If the state estimator performance needs to be pushed even further, state estimators that are not using linearization, such as the Unscented Kalman Filter, should be investigated.

Additional future work would be to investigate the effects of including the viscous forces, that come from the fact that the FoilCart is partly surrounded by water and partly by air, in the model. It may not come as a surprise that a watercraft model would benefit from more hydrodynamic components and depending on the speed, an aerodynamic analysis of the hull might also be necessary in the future.

When it comes to dynamic modelling of water, it can be argued that computational fluid dynamics (CFD) technology is superior to mechanical simplifications such as Simscape mechanical, used in [3]. A way to make use of CFD technology would be to generate lookup tables beforehand instead of computing the lift and drag equation in the loop. Not only could it increase the accuracy by making use of modern simulation technology, but also decreases the CPU utilization and minimize delays which is critical when operating a controller in real-time.

Implementation of aircraft control on a hydrofoil equipped watercraft would also be an interesting approach, as seen in Candela's latest hydrofoiling boat model, C-8 [2].

The wing dynamics can also be extended beyond the lift and drag equation since the forces on the wing depend on more than just the angle of attack.

Bibliography

- [1] “Hydrofoiling.” [Online]. Available: <https://sv.wikipedia.org/wiki/B%C3%A4rplansb%C3%A5t>
- [2] “The Candela C-8 - An unrivaled electric experience on the water.” [Online]. Available: <https://candela.com/candela-c-8/>
- [3] H. Strömqvist, “Robust motion control strategies for hydrofoil-equipped naval vessels considering scaling effects,” p. 94.
- [4] “Svjo, (CC) Creative Commons Attribution-ShareAlike 4.0 International.” [Online]. Available: <https://sv.wikipedia.org/wiki/Eulervinklar#/media/Fil:Euler-angles-1.png>
- [5] S. Krafes, Z. Chalh, and A. Saka, “Backstepping Controller Design for a 5 DOF Spherical Inverted Pendulum,” *International Journal of Engineering Research in Africa*, vol. 41, pp. 37–50, Feb. 2019. [Online]. Available: <https://www.scientific.net/JERA.41.37>
- [6] C. Zhang, H. Hu, D. Gu, and J. Wang, “Cascaded control for balancing an inverted pendulum on a flying quadrotor,” *Robotica*, vol. 35, no. 6, pp. 1263–1279, Jun. 2017. [Online]. Available: https://www.cambridge.org/core/product/identifier/S0263574716000035/type/journal_article
- [7] “Hydrofoil.” [Online]. Available: <https://www.thecanadianencyclopedia.ca/en/article/hydrofoil>
- [8] “America’s cup; ac75, the technology.” [Online]. Available: <https://www.americascup.com/the-technology>
- [9] “America’s cup; ac75, class rules.” [Online]. Available: <https://www.americascup.com/en/official/the-class-rule>
- [10] “Monoplane - Wikipedia.” [Online]. Available: <https://en.wikipedia.org/wiki/Monoplane>
- [11] E. Wan and R. Van Der Merwe, “The unscented Kalman filter for nonlinear estimation,” in *Proceedings of the IEEE 2000 Adaptive Systems for Signal Processing, Communications, and Control Symposium (Cat. No.00EX373)*. Lake Louise, Alta., Canada: IEEE, 2000, pp. 153–158. [Online]. Available: <http://ieeexplore.ieee.org/document/882463/>
- [12] “Extended kalman filter.” [Online]. Available: https://en.wikipedia.org/wiki/Extended_Kalman_filter
- [13] F. Haugen, “Derivation of a Discrete-Time Lowpass Filter,” p. 3.

- [14] “Discretization.” [Online]. Available: https://users.wpi.edu/~zli11/teaching/rbe595_2017/LectureSlide_PDF/discretization.pdf
- [15] F. Gustafsson and A. Isaksson, “Best choice of coordinate system for tracking coordinated turns,” in *Proceedings of 35th IEEE Conference on Decision and Control*, vol. 3. Kobe, Japan: IEEE, 1996, pp. 3145–3150. [Online]. Available: <http://ieeexplore.ieee.org/document/573612/>
- [16] “Datasheet accelerometer and gyroscope stm300.” [Online]. Available: <https://sensor.azurewebsites.net/media/5z5lv25o/ts1524-r28-datasheet-stm300.pdf>
- [17] “The Lift Equation.” [Online]. Available: <https://www.grc.nasa.gov/www/k-12/airplane/lifteq.html>
- [18] “The Drag Equation.” [Online]. Available: <https://www.grc.nasa.gov/www/k-12/airplane/drageq.html>

